Rare glutamic acid methyl ester peptaibols from *Sepedonium ampullosporum* Damon KSH 534 exhibit promising anticancer activity

Yen T. H. Lam [1,2], Manuel G. Ricardo [1,3], Robert Rennert [1], Andrej Frolov [1,4], Andrea Porzel [1], Wolfgang Brandt [1], Pauline Stark [1], Bernhard Westermann [1] and Norbert Arnold [1,*]

1 Department of Bioorganic Chemistry, Leibniz Institute of Plant Biochemistry, Weinberg 3, D-06120 Halle (Saale), Germany; ThiHaiYen.Lam@ipb-halle.de (Y.T.H.L.); Robert.Rennert@ipb-halle.de (R.R.); Andrej.Frolov@ipb-halle.de (A.F.); Andrea.Porzel@ipb-halle.de (A.P.); Wolfgang.Brandt@ipb-halle.de (W.B.); Pauline.Stark@ipb-halle.de (P.S.); Bernhard.Westermann@ipb-halle.de (B.W.); Norbert.Arnold@ipb-halle.de (N.A.)

2 Department of Organic Chemistry, Faculty of Chemistry, Hanoi National University of Education, 136 Xuanthuy, Caugiay, Hanoi, Vietnam;

3 Department of Biomolecular Systems, Max Planck Institute of Colloids and Interfaces, Am Mühlenberg 1, D-14476 Potsdam, Germany; Manuel.GarciaRicardo@mpikg.mpg.de (M.G.R.)

4 Department of Biochemistry, Faculty of Biology, St. Petersburg State University, Sredny Prospekt V.O. 41, 199004, St. Petersburg, Russian Federation;

* Correspondence: Norbert.Arnold@ipb-halle.de; Tel.: +49-345-5582-1310

Supplementary Materials

Table of contents

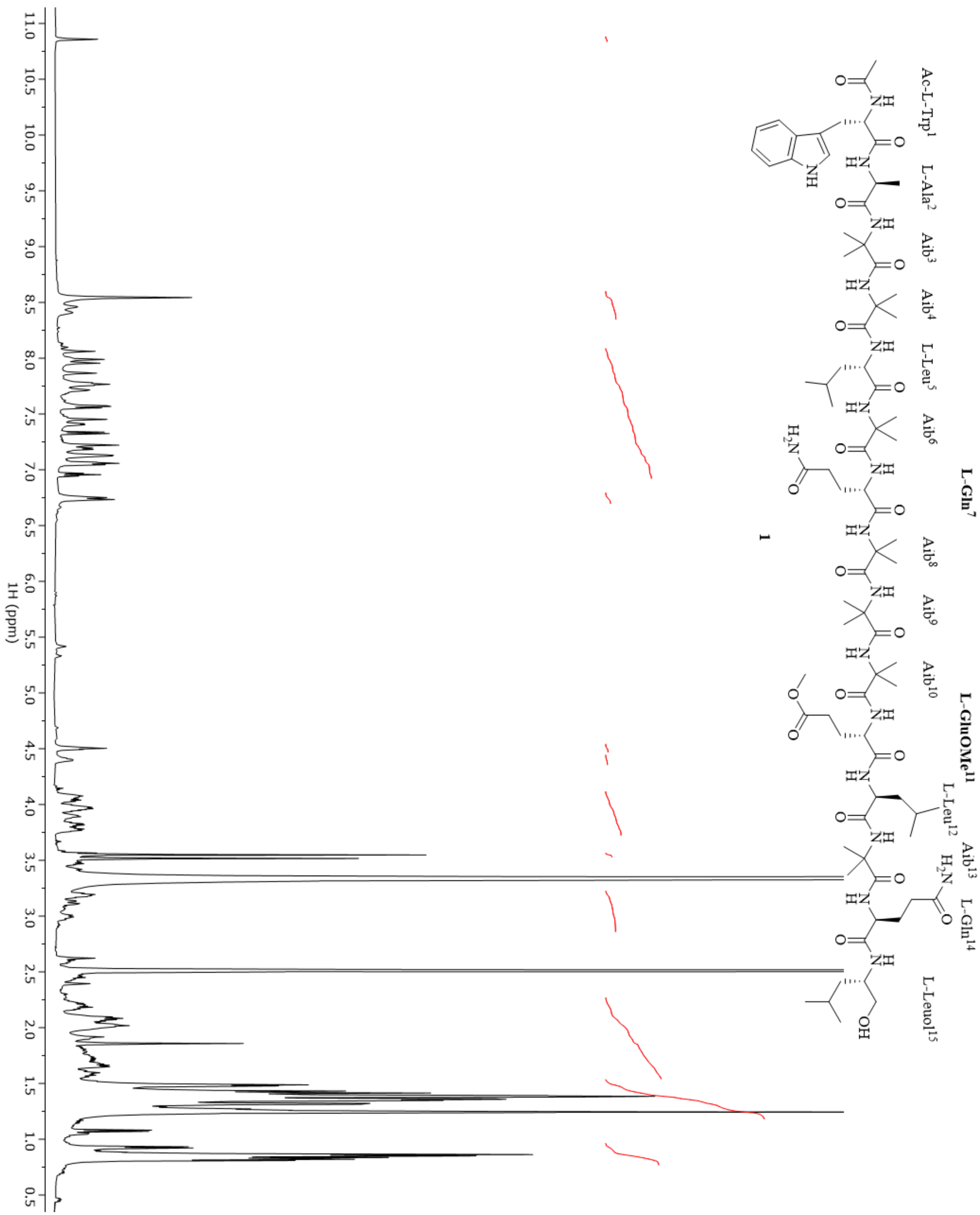

Figure S1. [1]H NMR spectrum of natural ampullosporin F (**1**) (600 MHz, DMSO-*d*6).

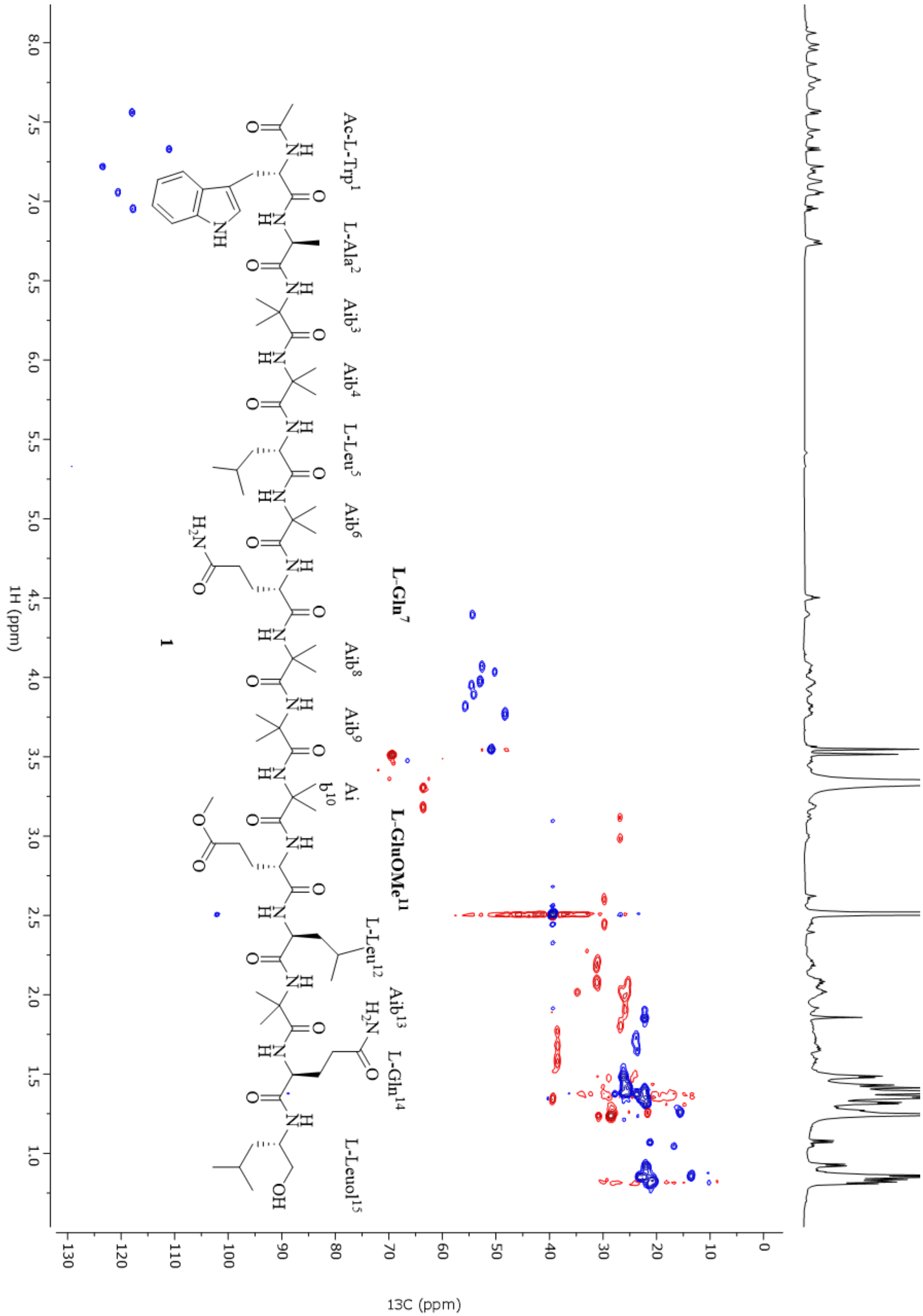

Figure S2. [1]H, [13]C HSQC spectrum of natural ampullosporin F (**1**) (600 MHz, DMSO-d_6).

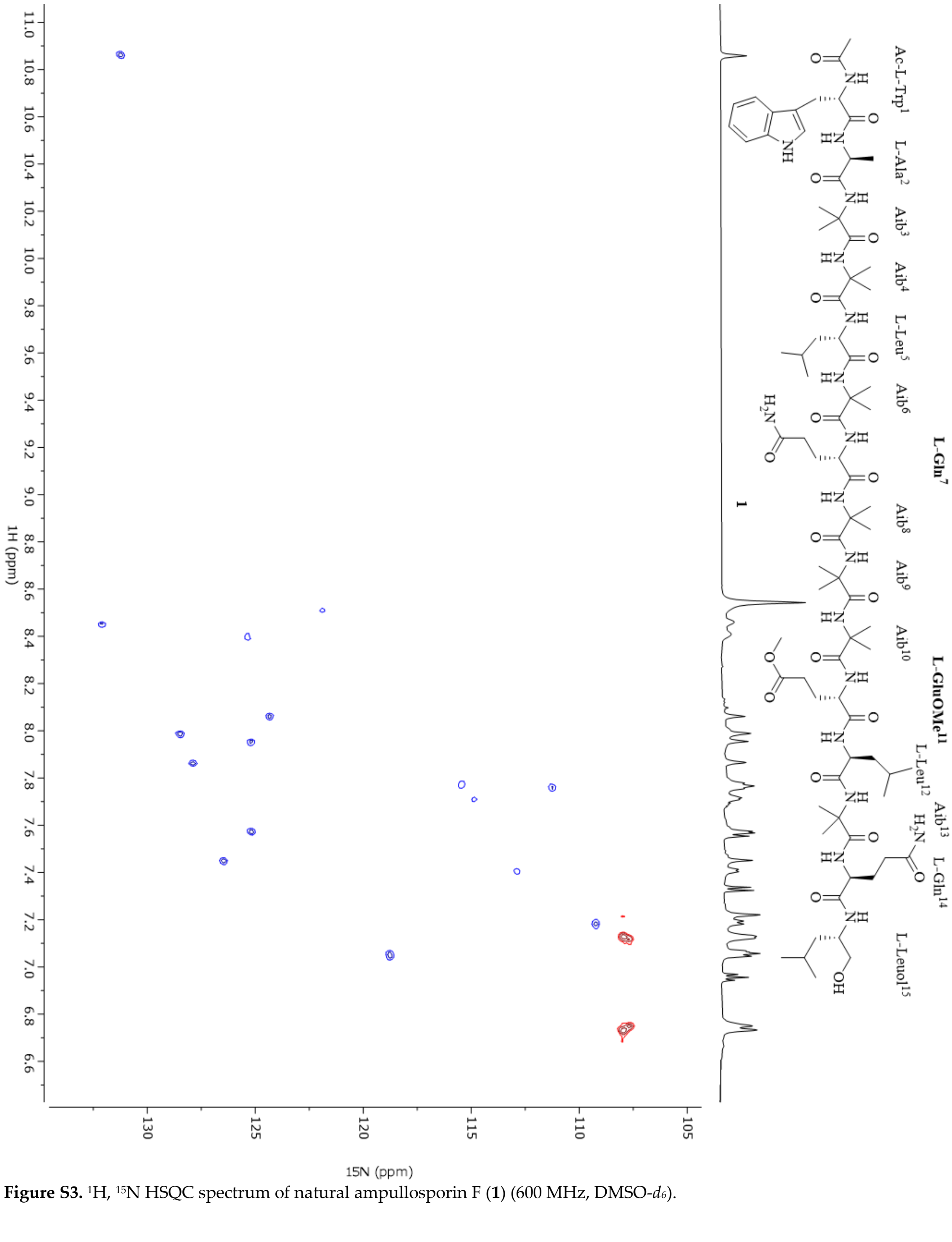

Figure S3. ^{1}H, ^{15}N HSQC spectrum of natural ampullosporin F (**1**) (600 MHz, DMSO-d_6).

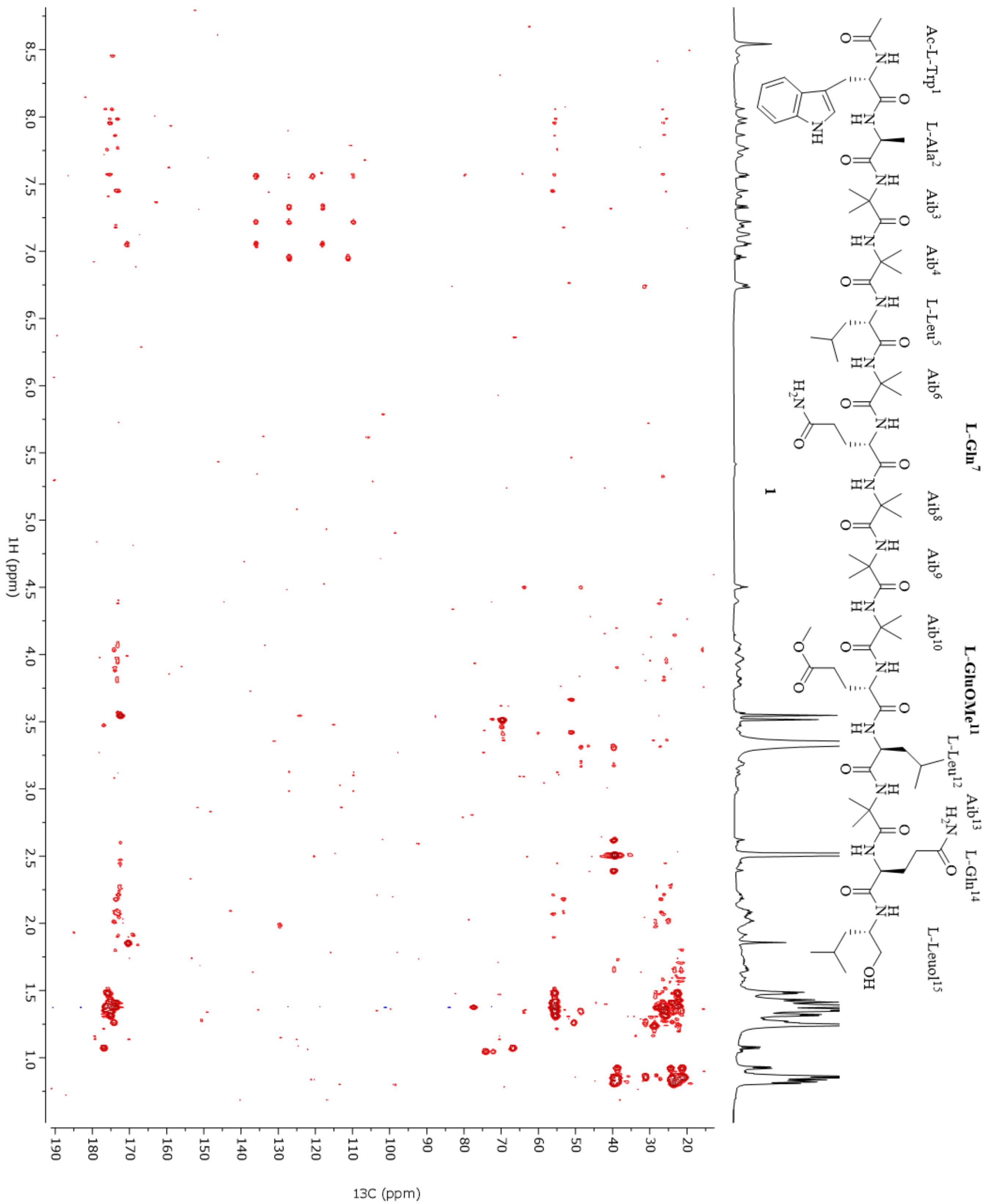

Figure S4. ^{1}H, ^{13}C HMBC spectrum of natural ampullosporin F (**1**) (600 MHz, DMSO-d_6).

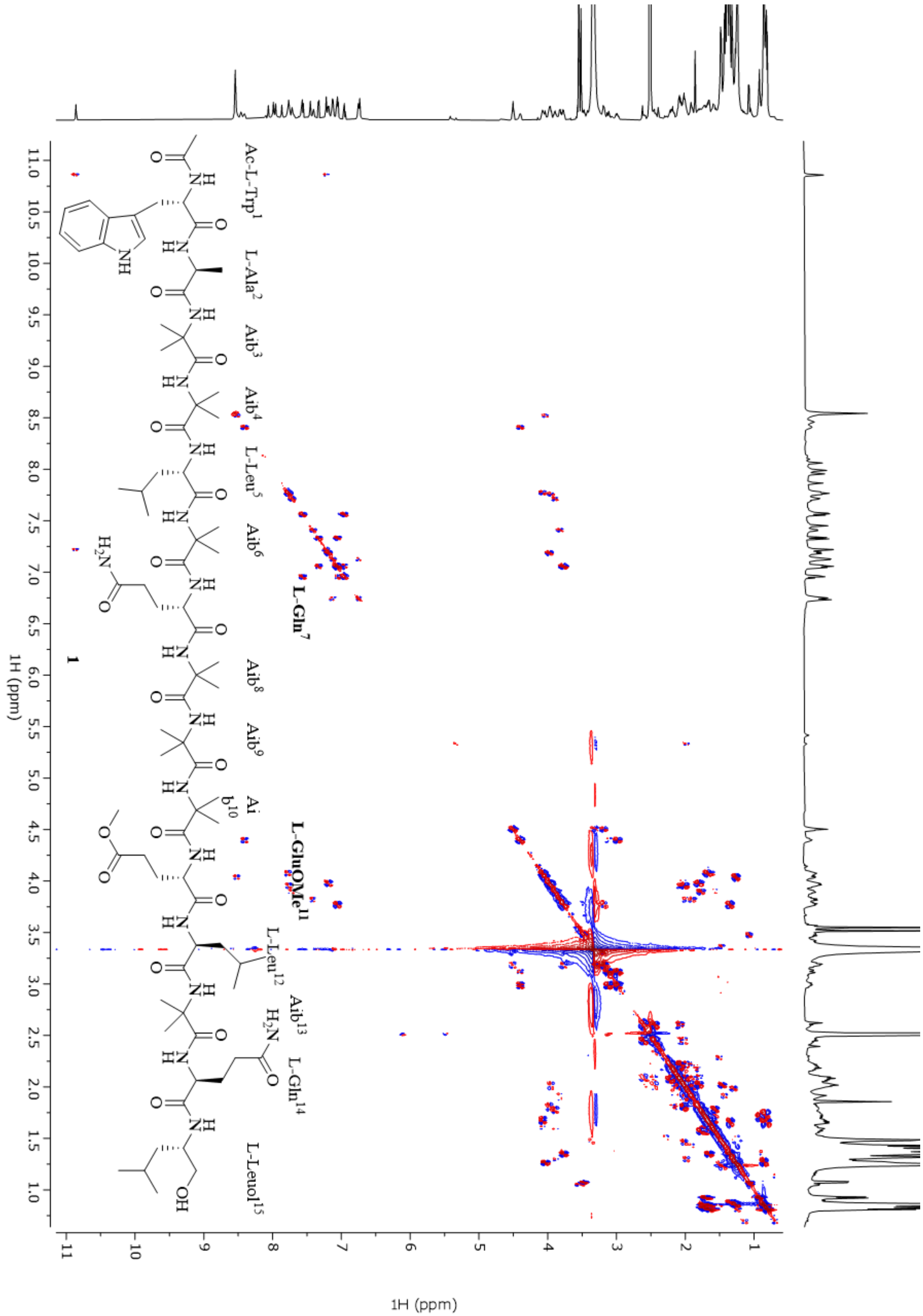

Figure S5. ^{1}H, ^{1}H COSY spectrum of natural ampullosporin F (**1**) (600 MHz, DMSO-d_6).

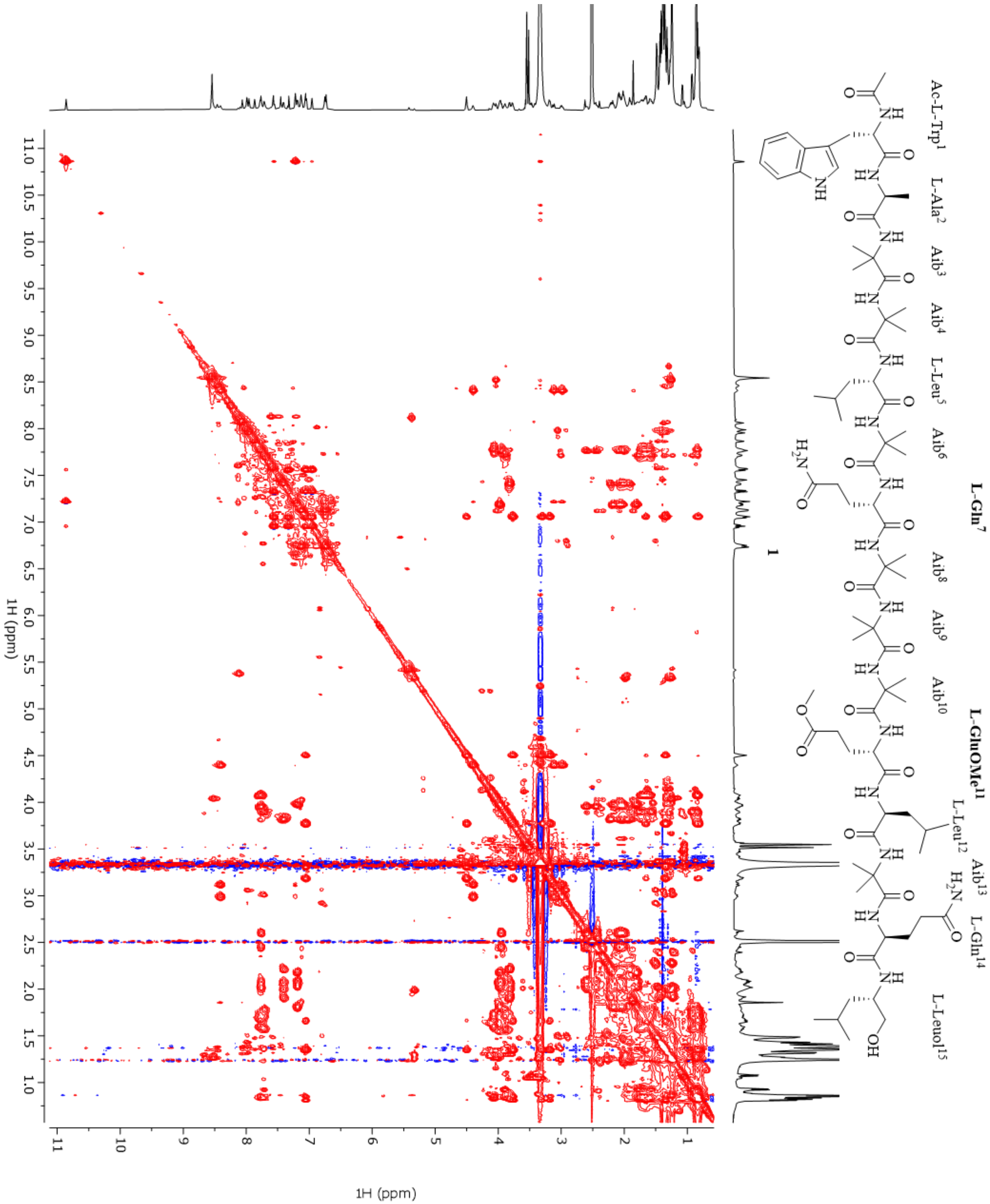

Figure S6. ^{1}H, ^{1}H TOCSY spectrum of natural ampullosporin F (**1**) (600 MHz, DMSO-d_6).

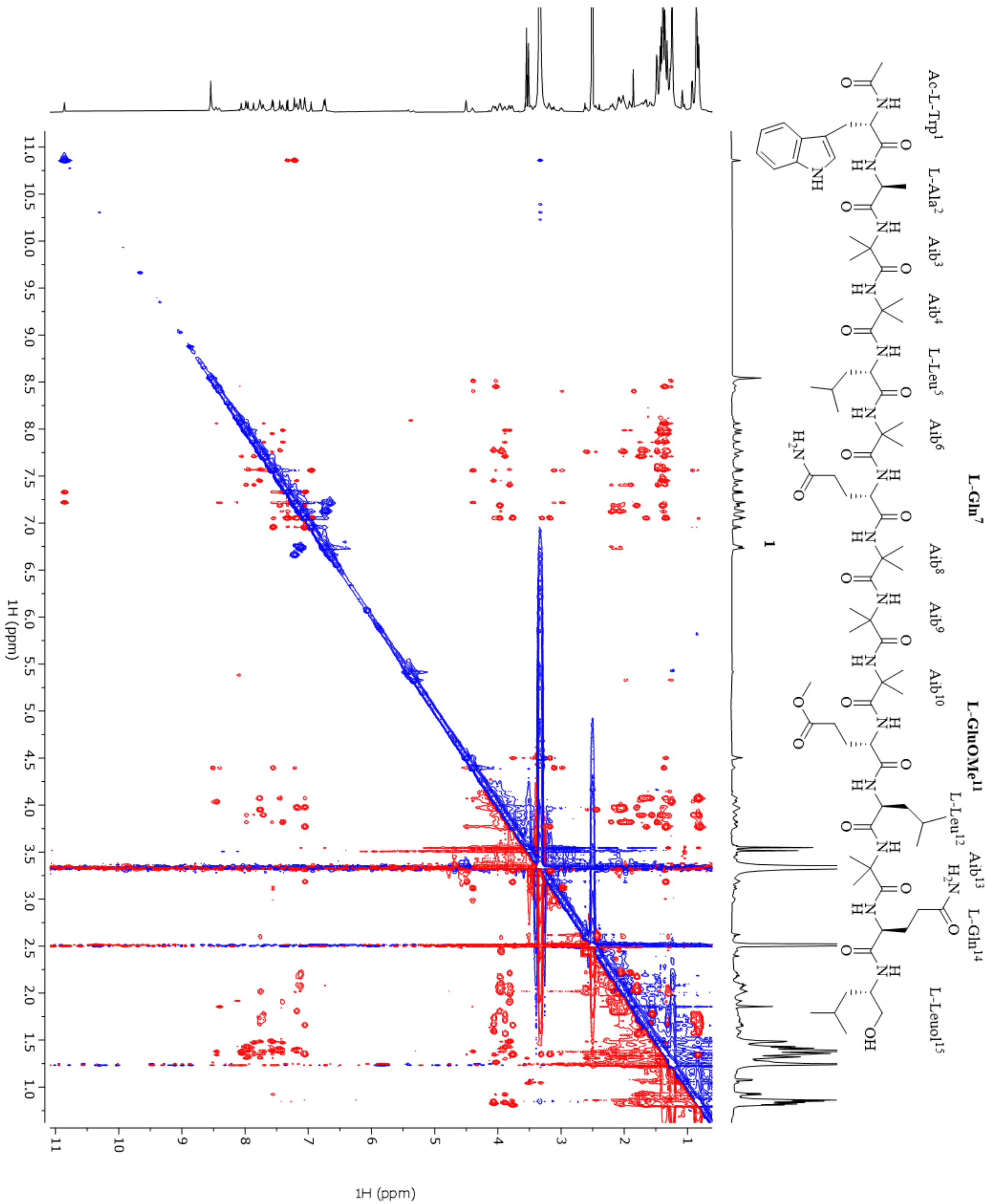

Figure S7. ^{1}H, ^{1}H ROESY spectrum of natural ampullosporin F (**1**) (600 MHz, DMSO-d_6).

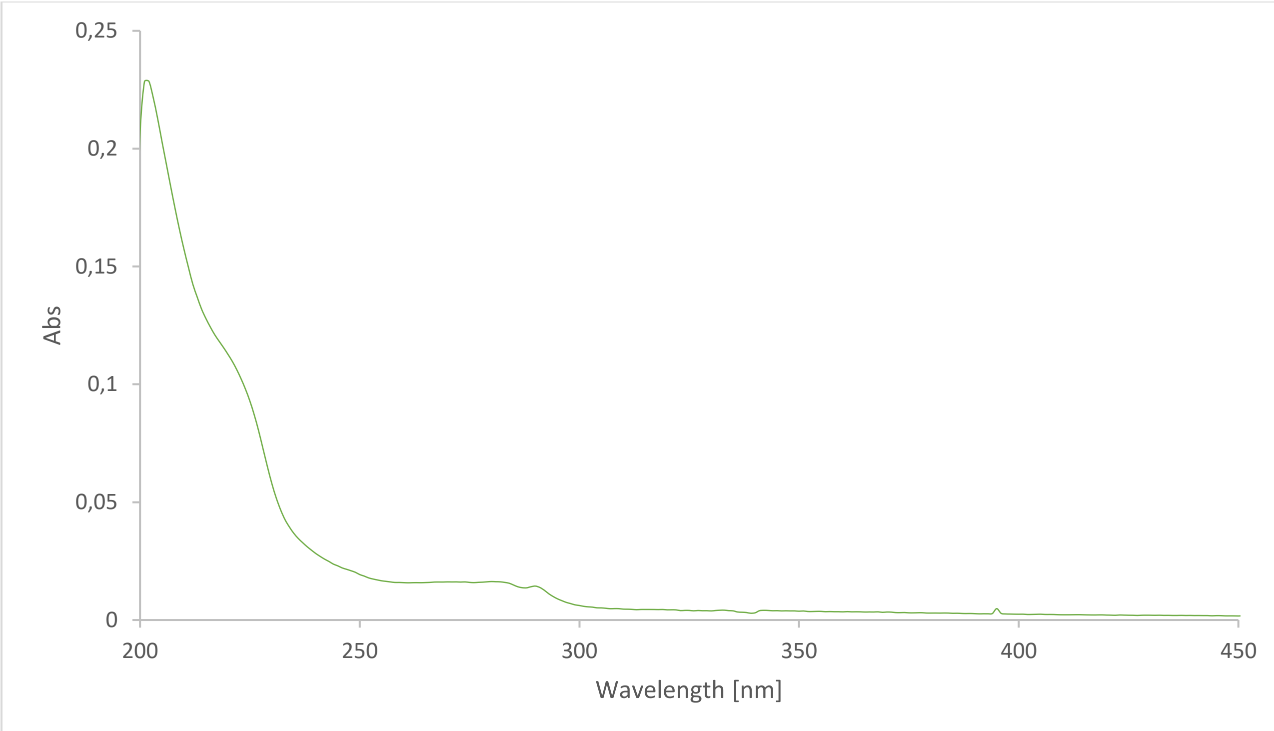

Figure S8. UV spectrum of natural ampullosporin F (**1**) in MeOH.

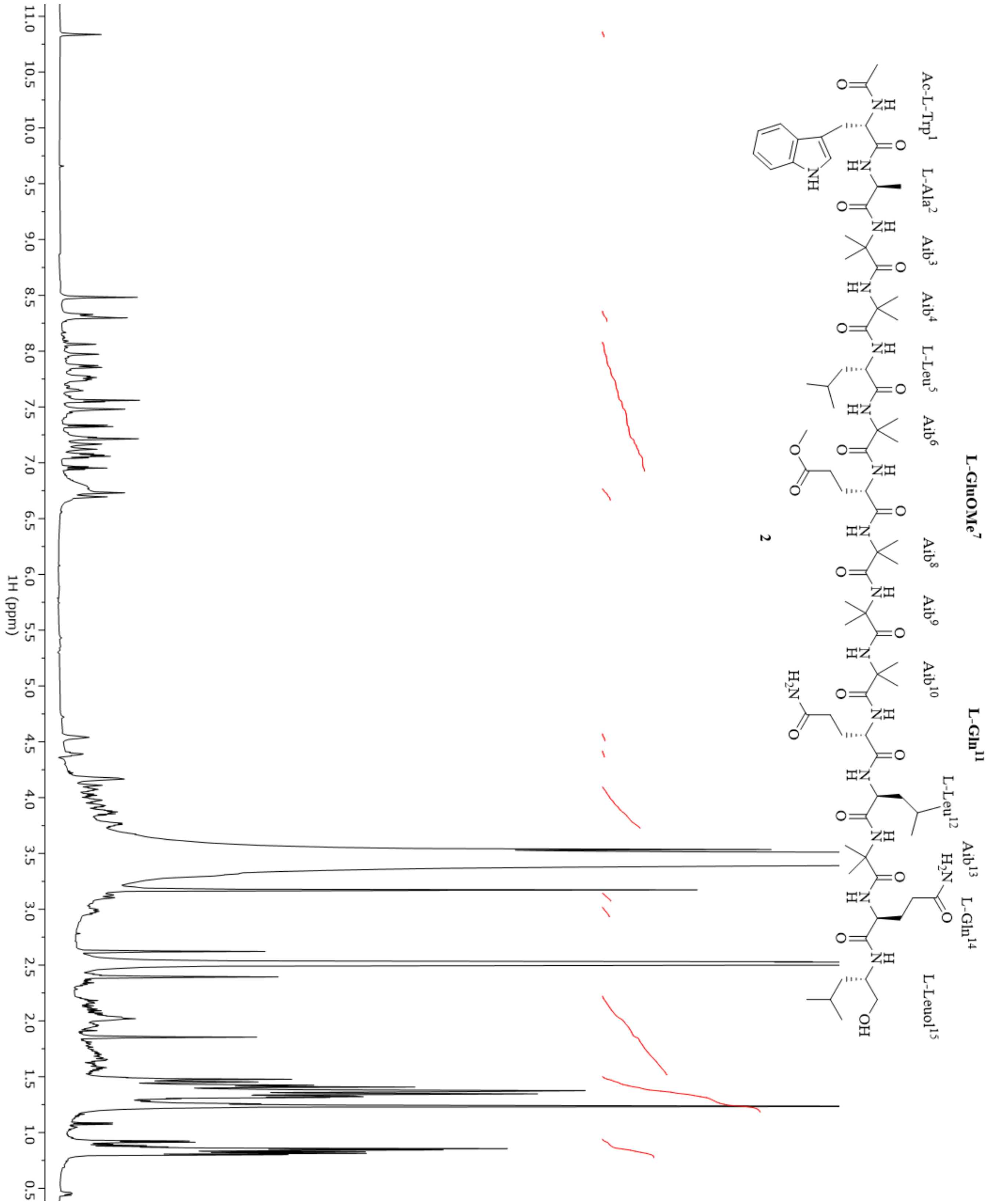

Figure S9. ^{1}H NMR spectrum of natural ampullosporin G (**2**) (600 MHz, DMSO-d_6).

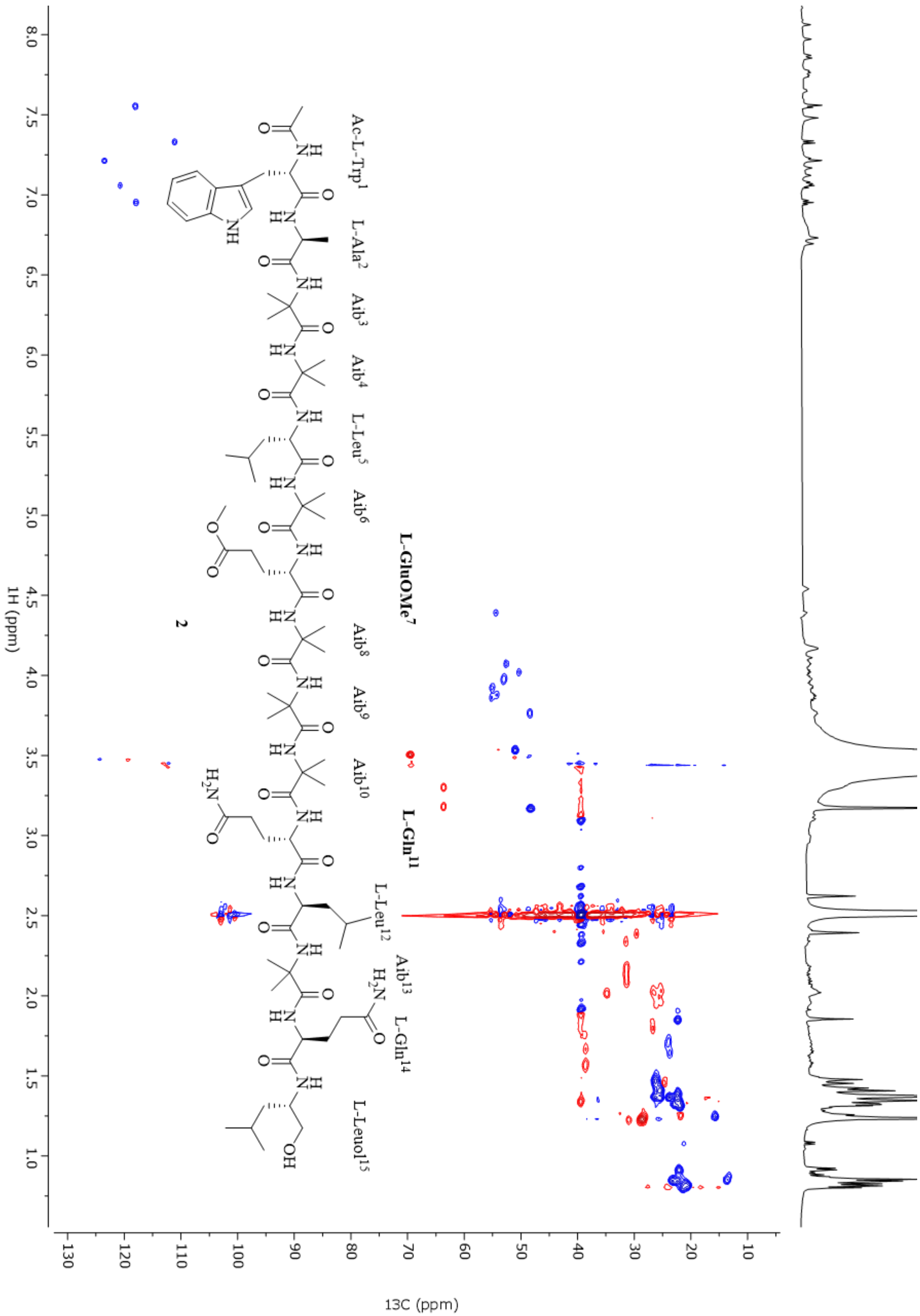

Figure S10. ^{1}H, ^{13}C HSQC spectrum of natural ampullosporin G (**2**) (600 MHz, DMSO-d_6).

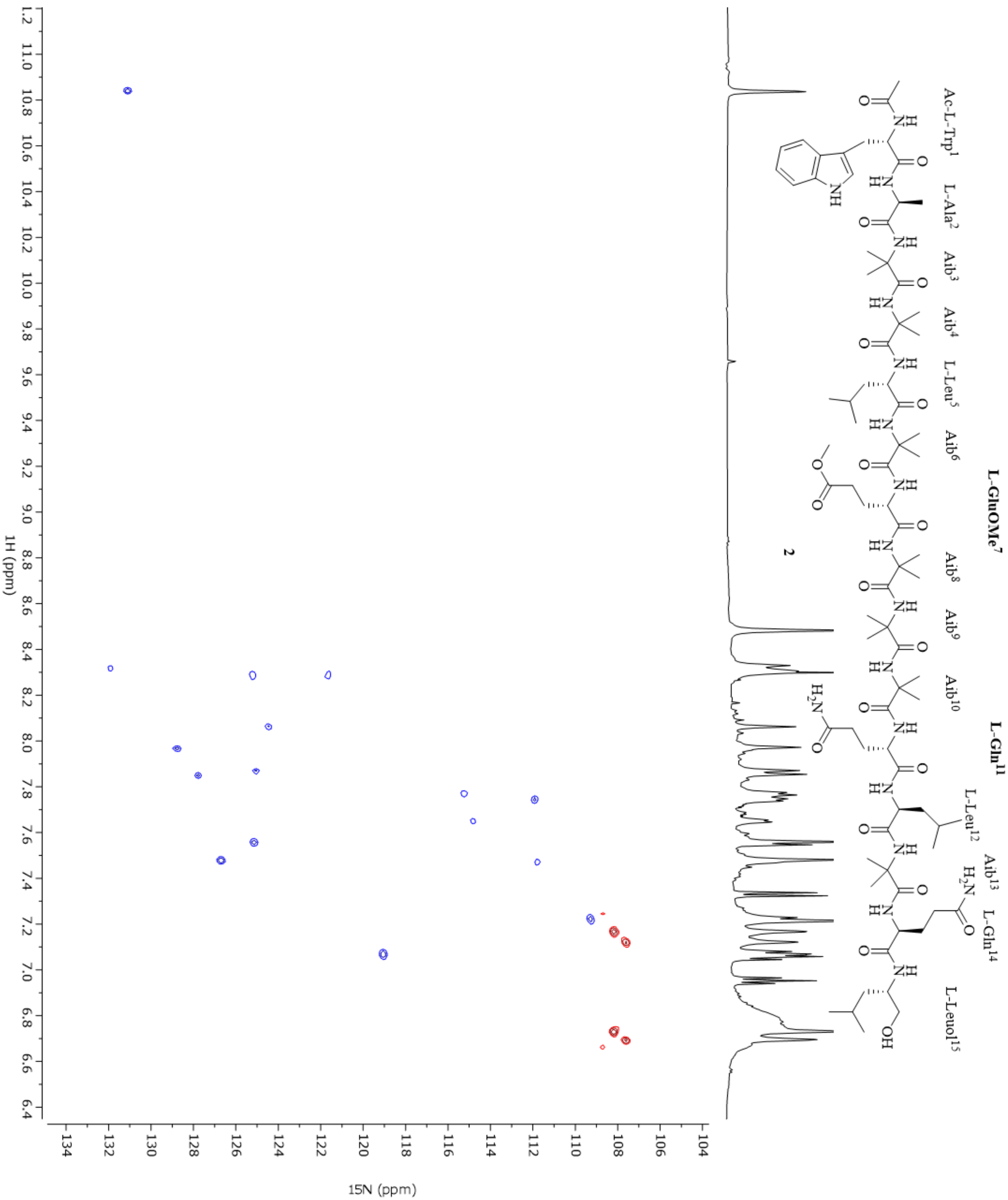

Figure S11. ^{1}H, ^{15}N HSQC spectrum of natural ampullosporin G (**2**) (600 MHz, DMSO-d_6).

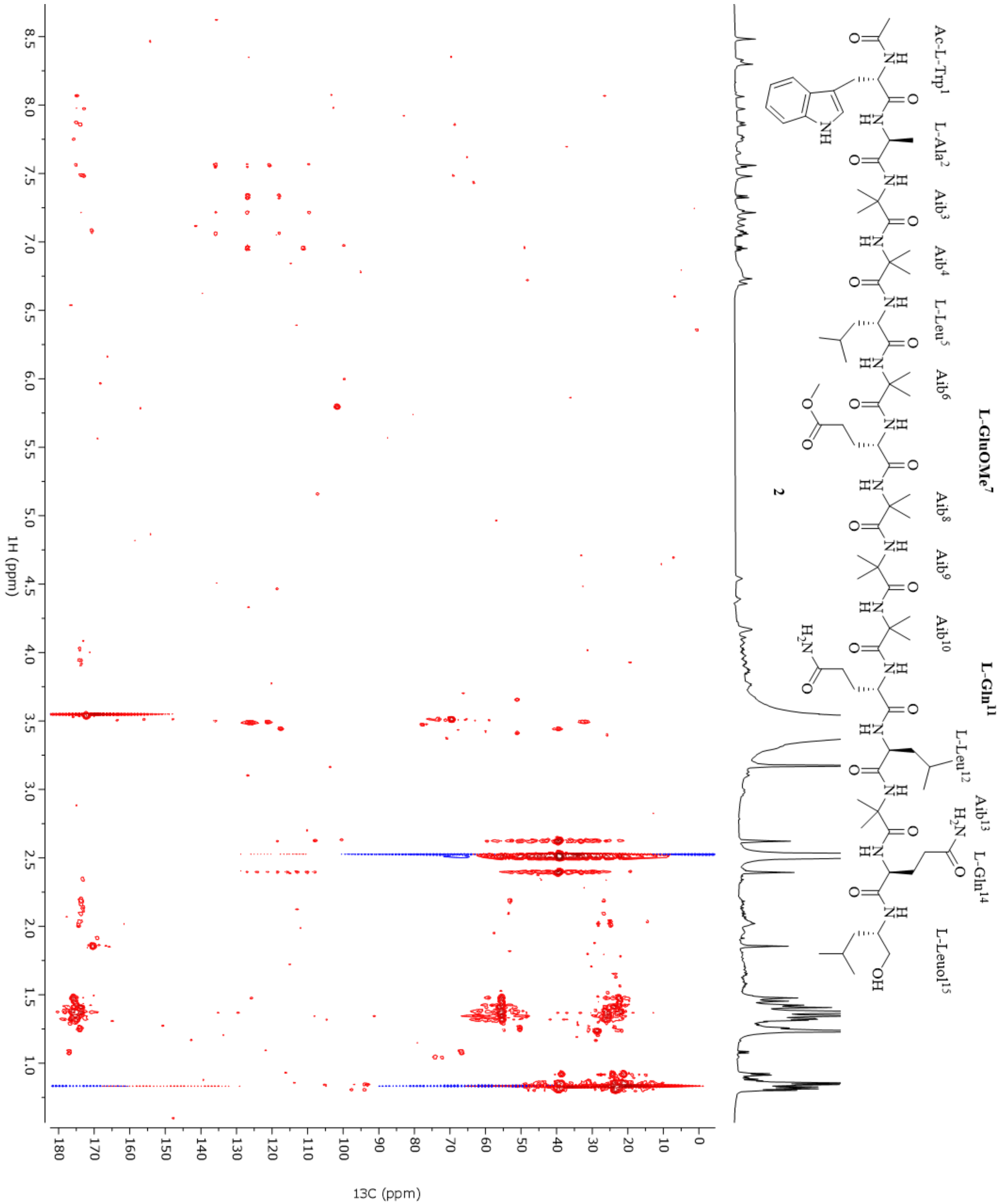

Figure S12. ^{1}H, ^{13}C HMBC spectrum of natural ampullosporin G (**2**) (600 MHz, DMSO-d_6).

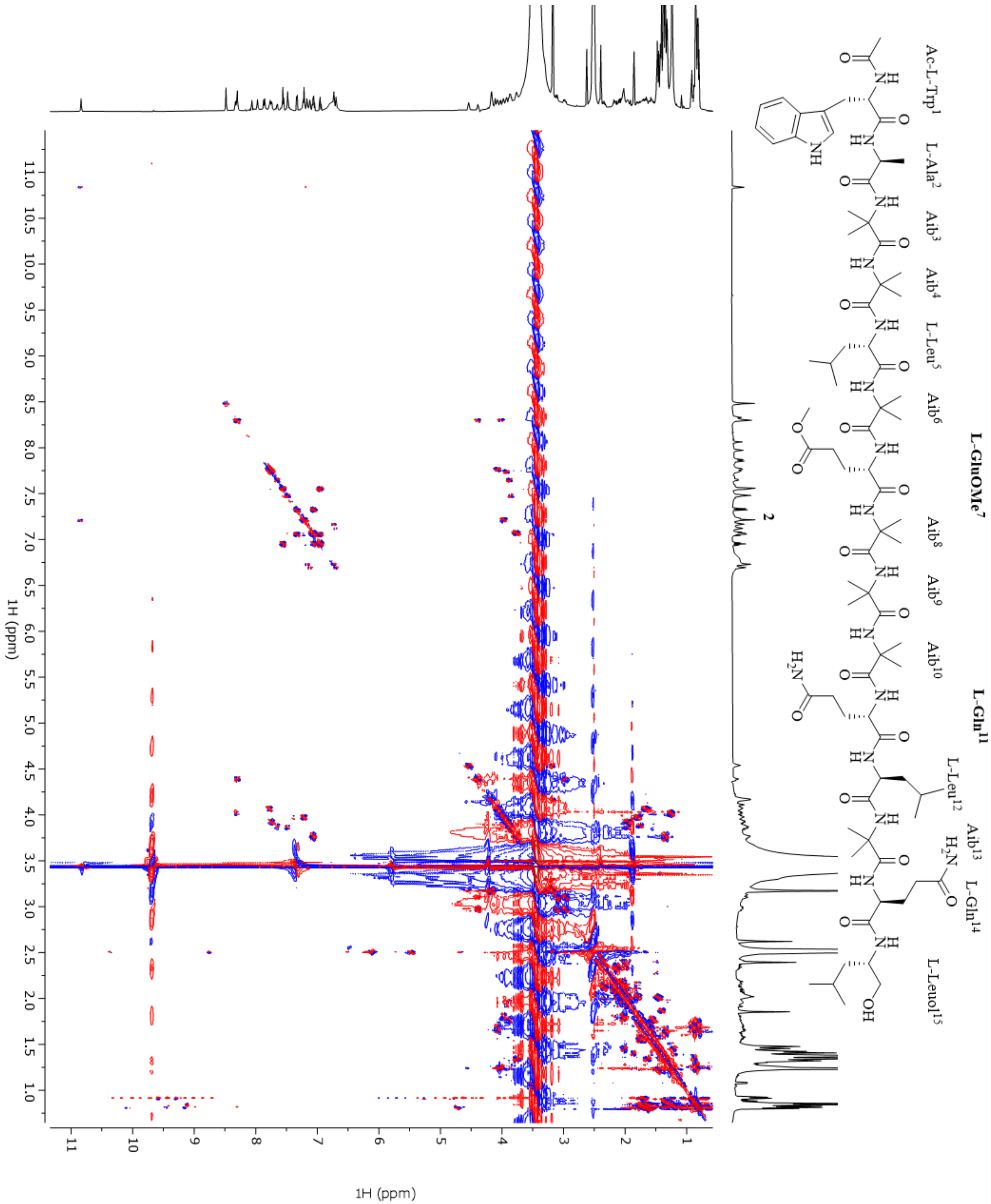

Figure S13. ^{1}H, ^{1}H COSY spectrum of natural ampullosporin G (**2**) (600 MHz, DMSO-d_6).

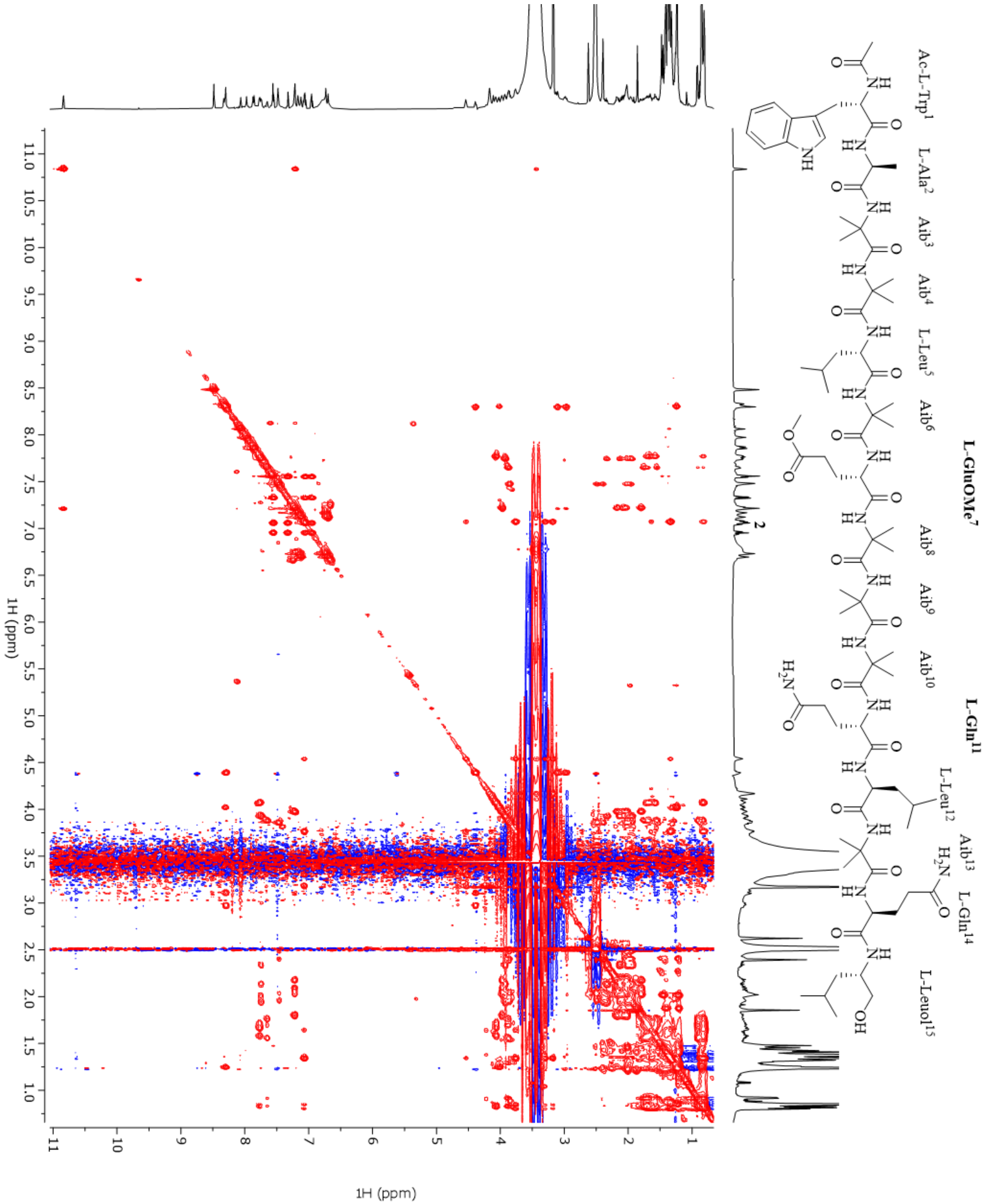

Figure S14. ^{1}H, ^{1}H TOCSY spectrum of natural ampullosporin G (**2**) (600 MHz, DMSO-d_6).

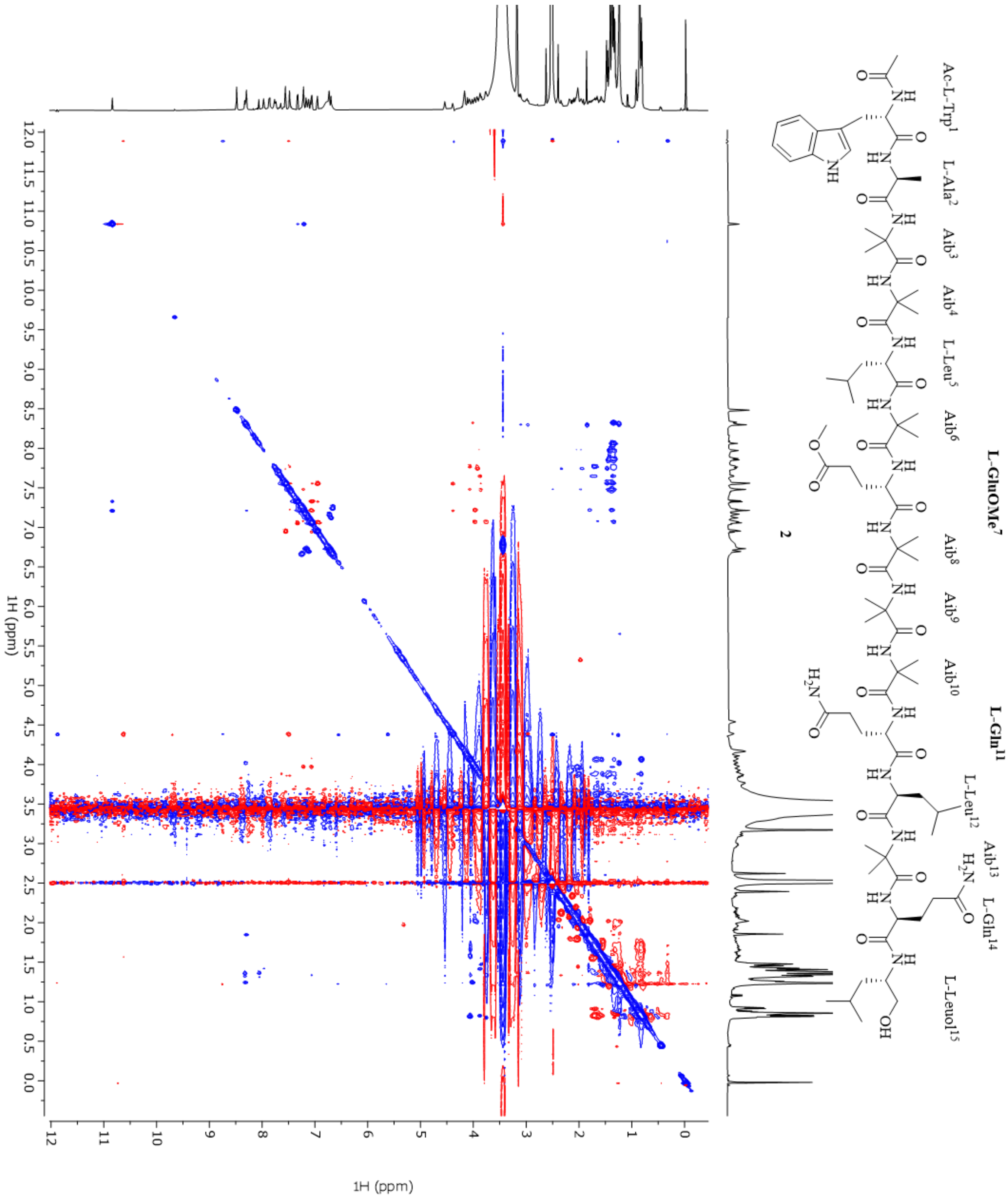

Figure S15. ^{1}H, ^{1}H ROESY spectrum of natural ampullosporin G (**2**) (600 MHz, DMSO-d_6).

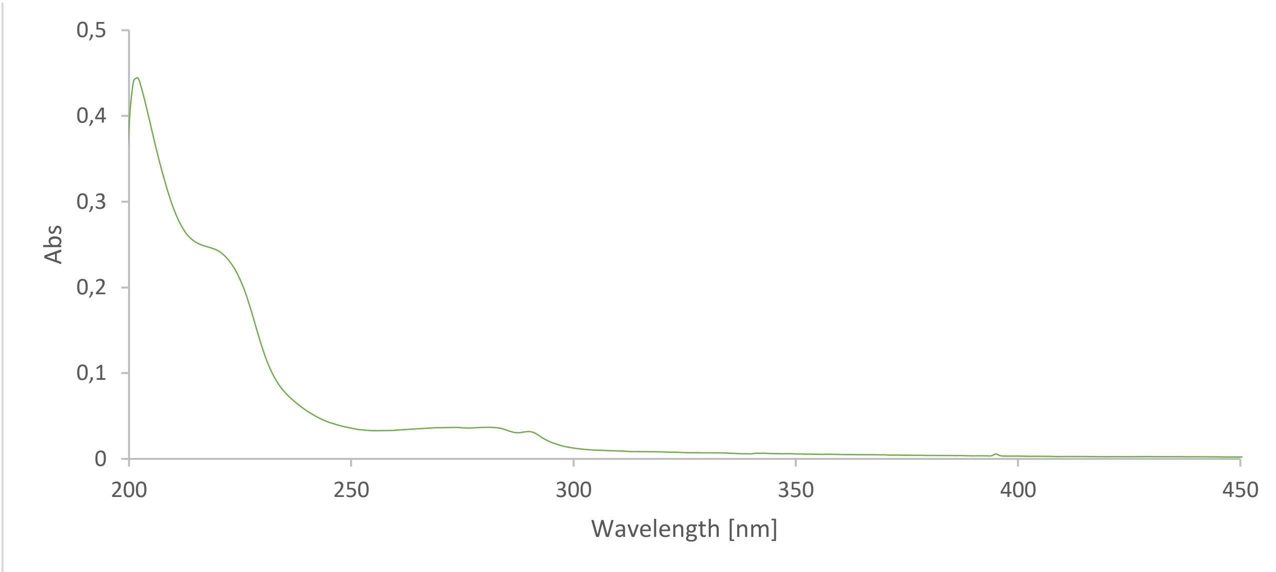

Figure S16. UV spectrum of natural ampullosporin G (**2**) in MeOH.

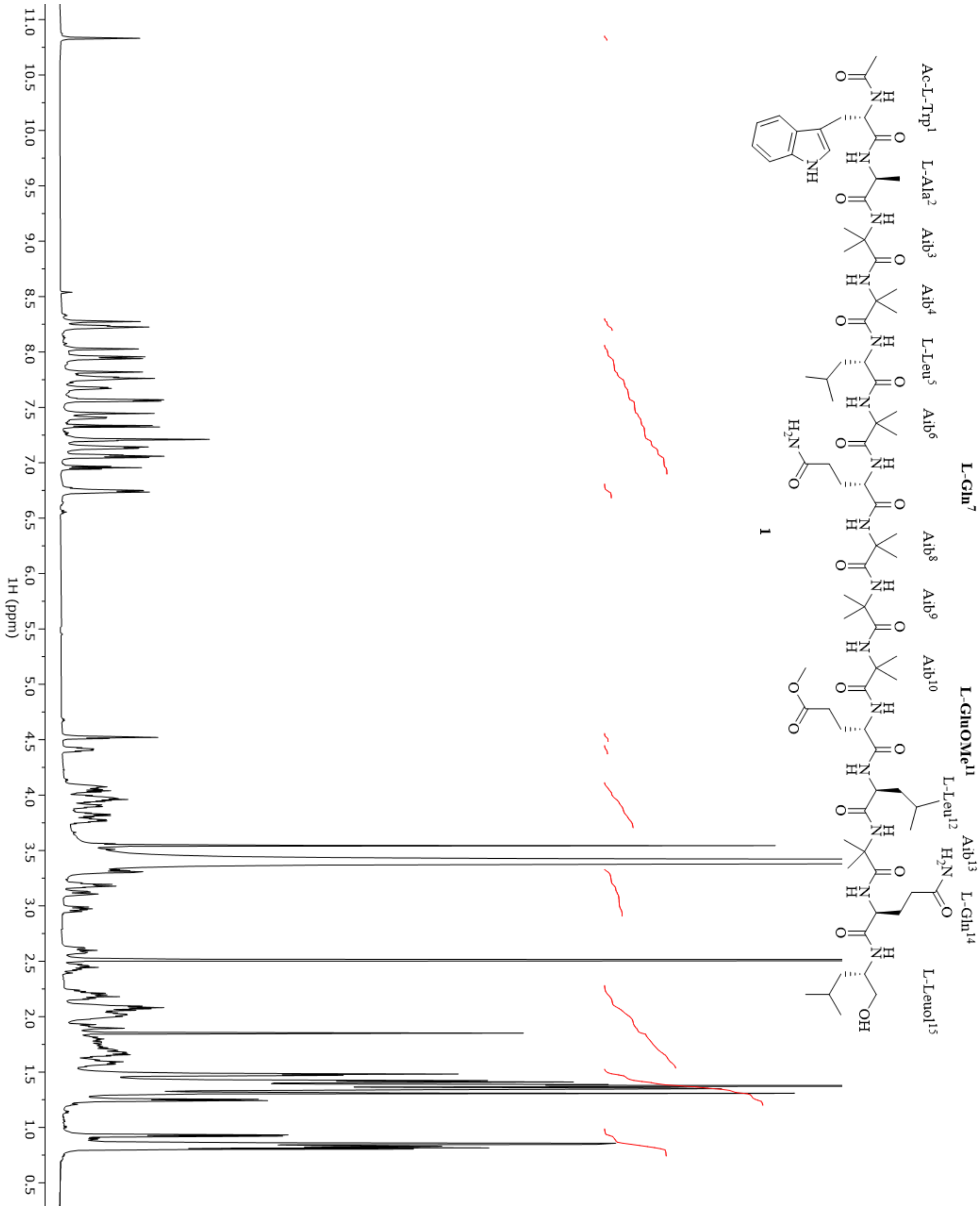

Figure S17. ^{1}H NMR spectrum of synthetic ampullosporin F (**1**) (600 MHz, DMSO-d_6).

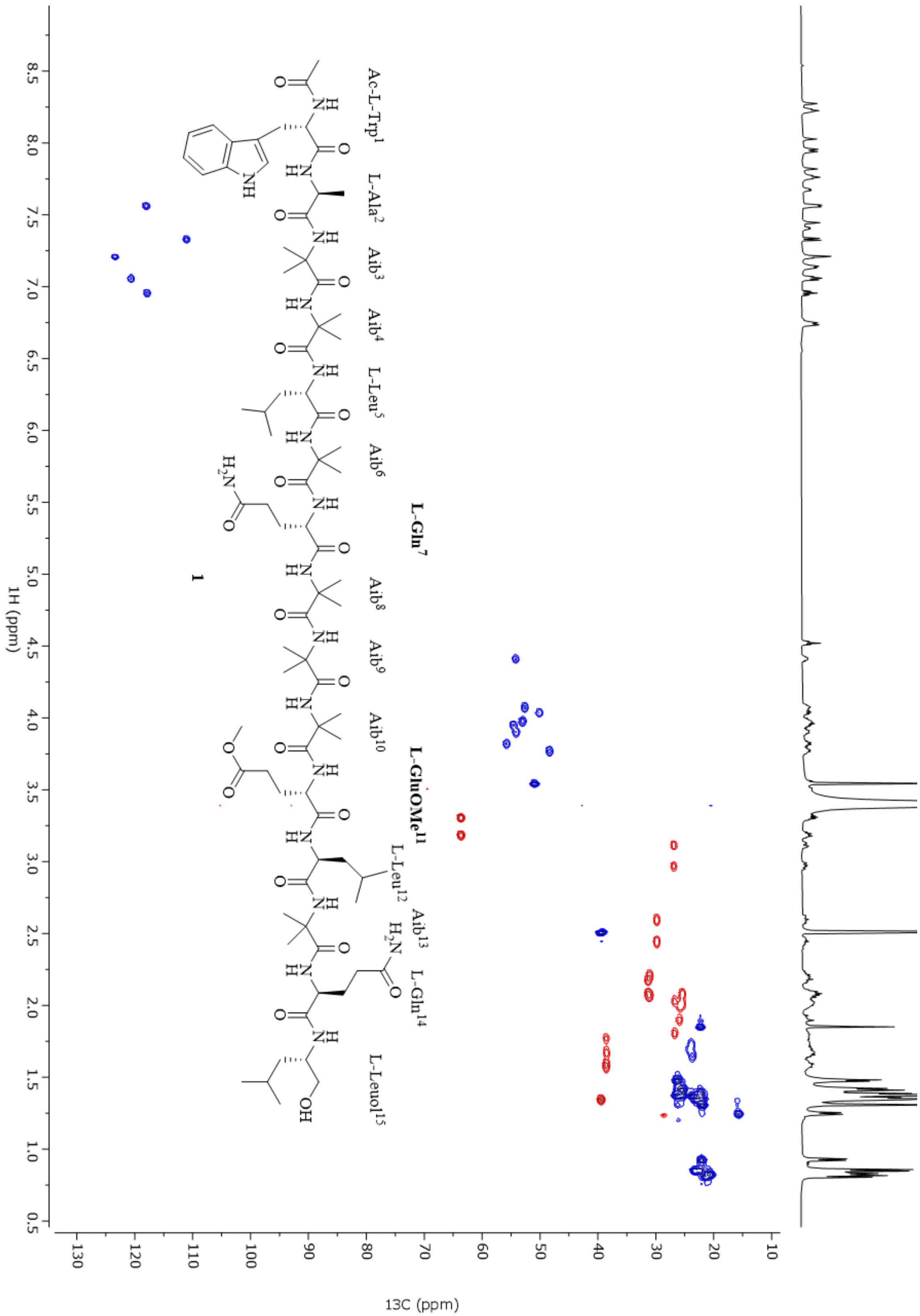

Figure S18. ^{1}H, ^{13}C HSQC spectrum of synthetic ampullosporin F (**1**) (600 MHz, DMSO-d_6).

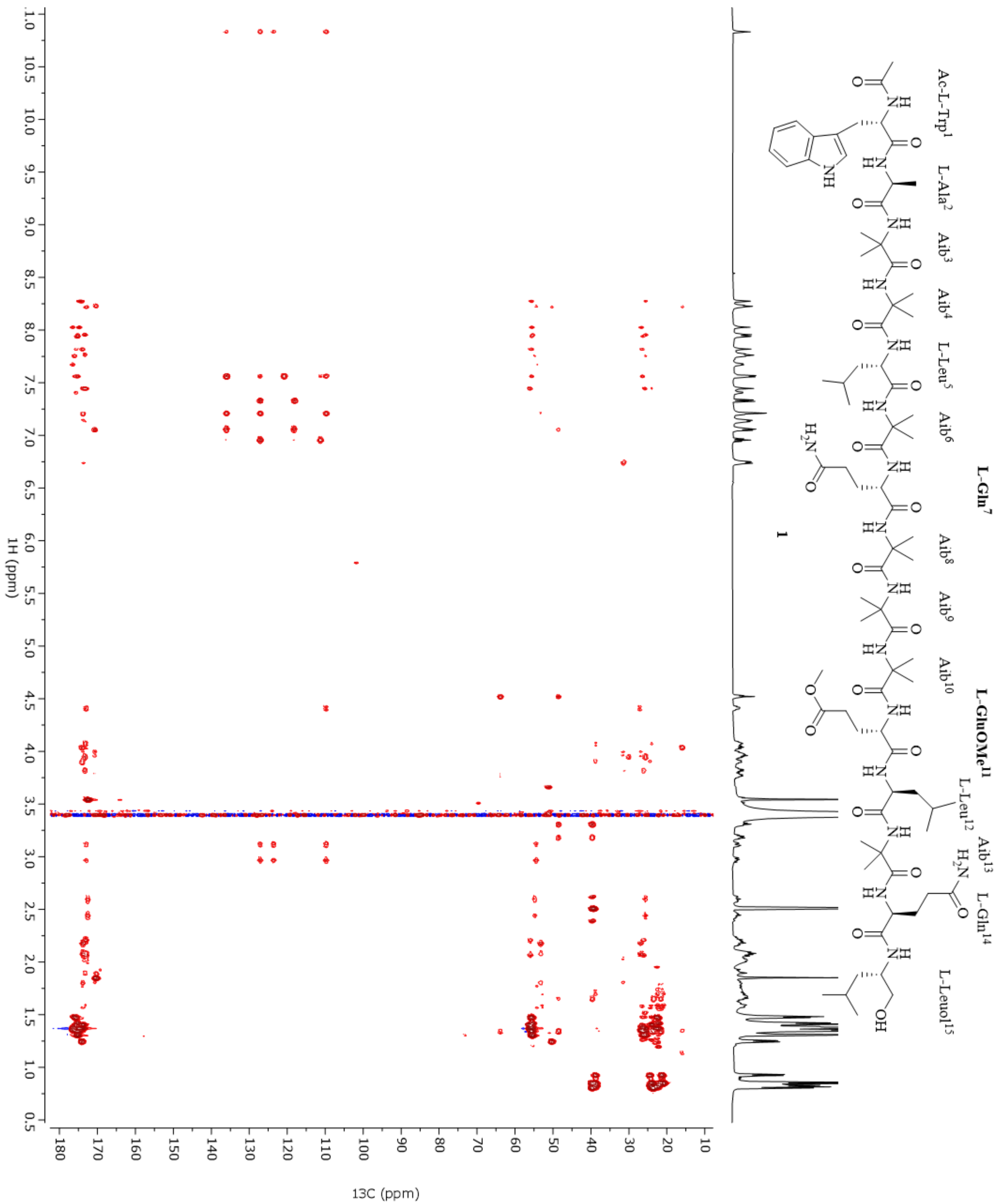

Figure S19. ^{1}H, ^{13}C HMBC spectrum of synthetic ampullosporin F (**1**) (600 MHz, DMSO-d_6).

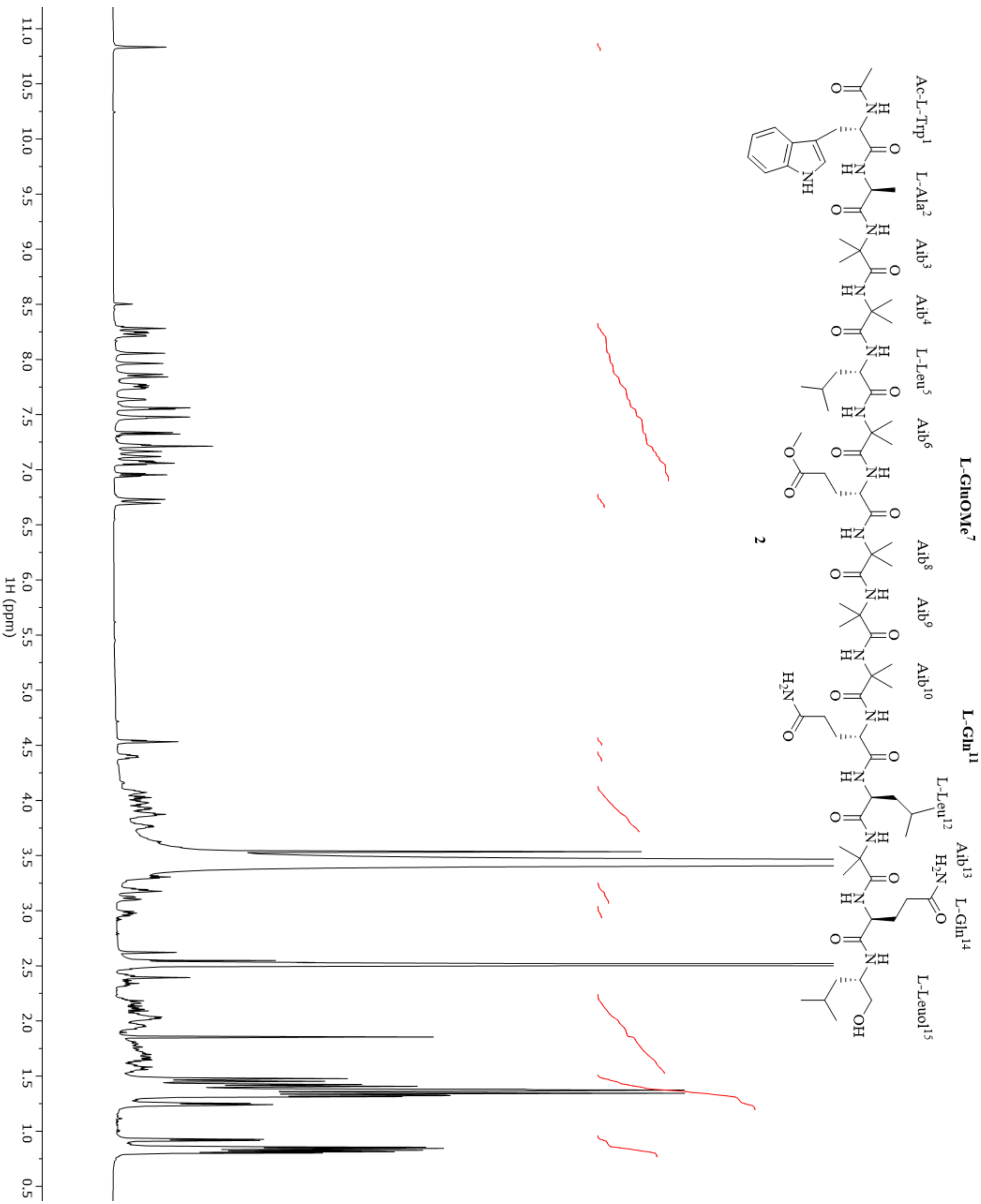

Figure S20. ^1H NMR spectrum of synthetic ampullosporin G (**2**) (600 MHz, DMSO-d_6).

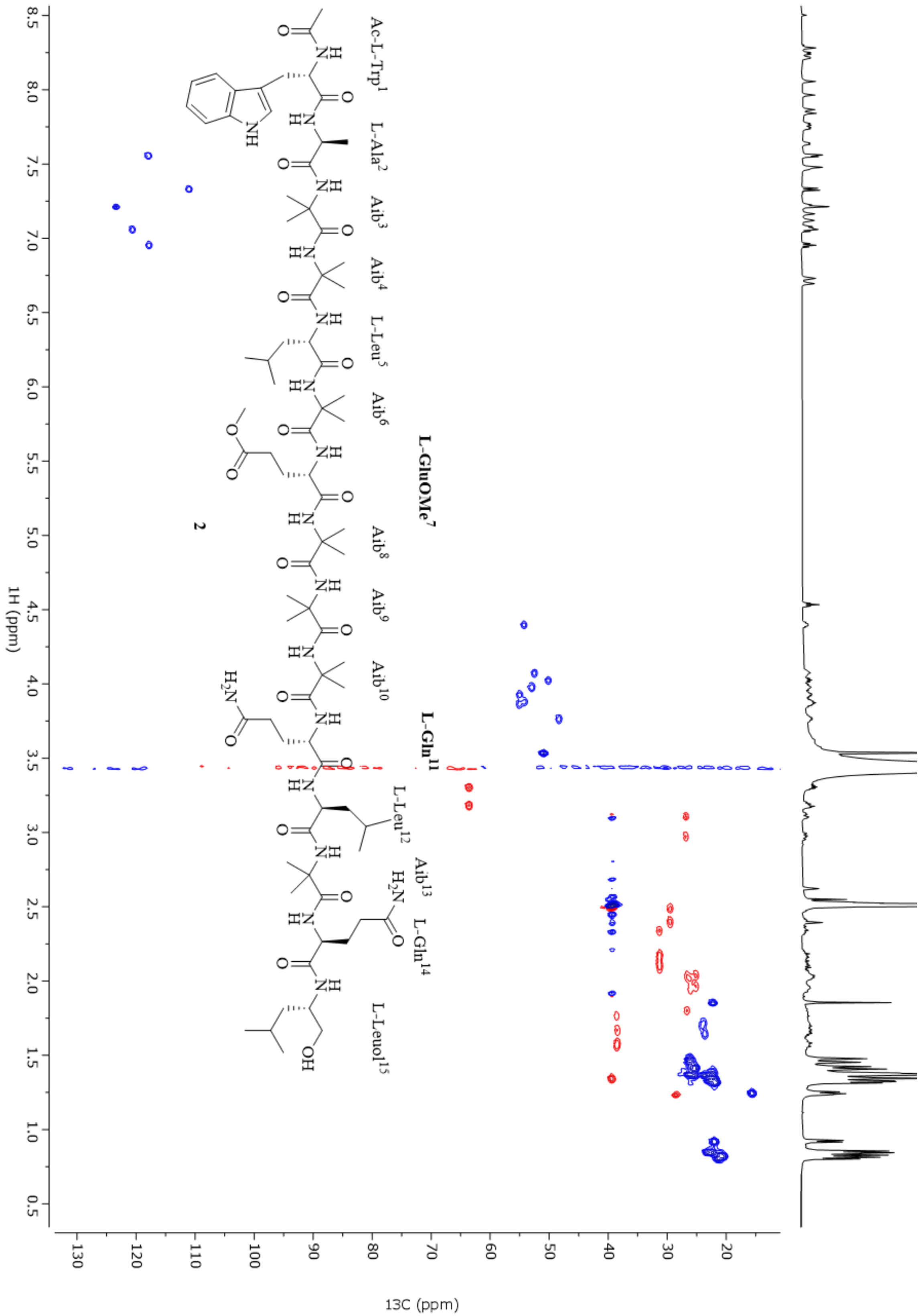

Figure S21. ^{1}H, ^{13}C HSQC spectrum of synthetic ampullosporin G (**2**) (600 MHz, DMSO-d_6).

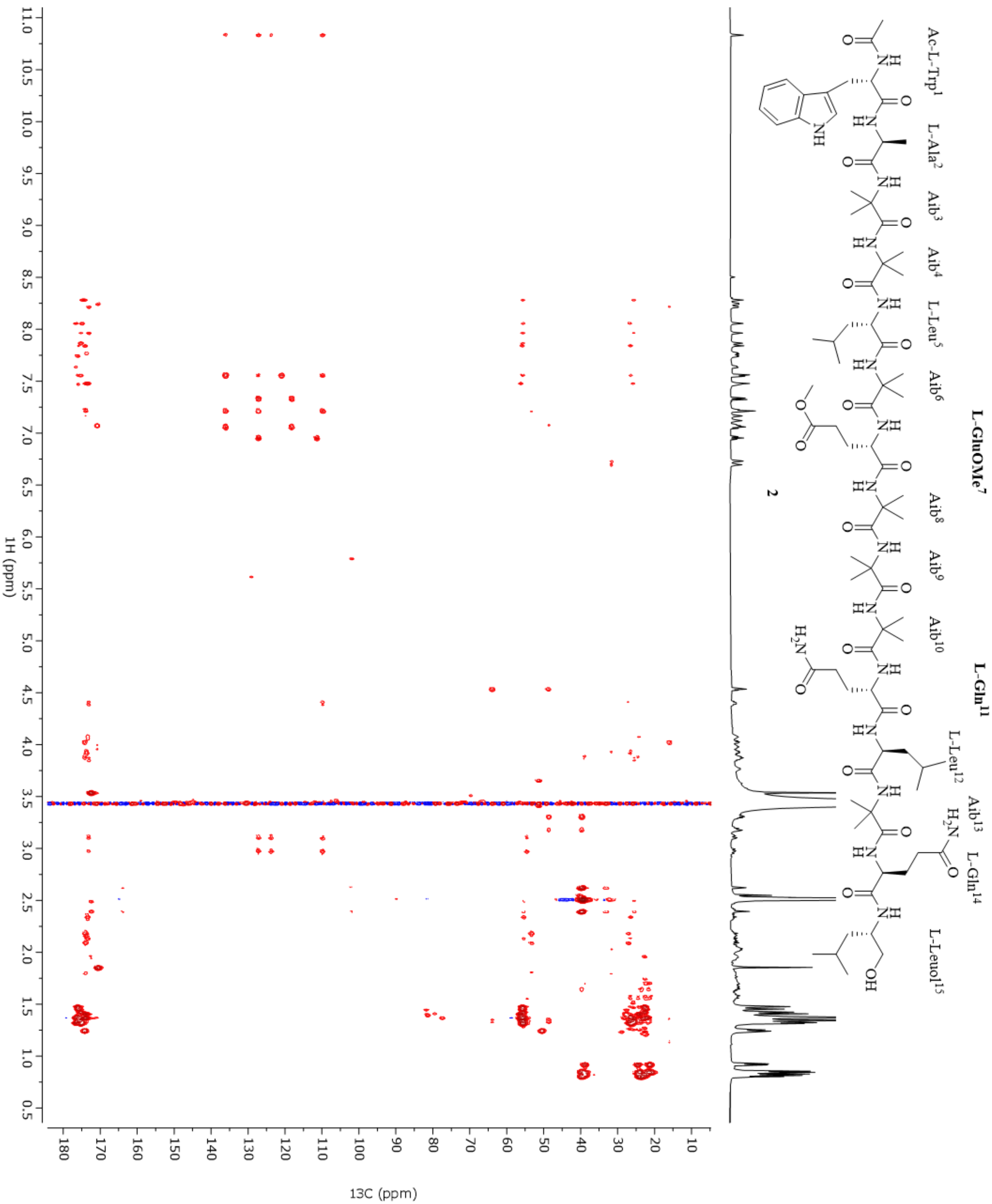

Figure S22. ^{1}H, ^{13}C HMBC spectrum of synthetic ampullosporin G (**2**) (600 MHz, DMSO-d_6).

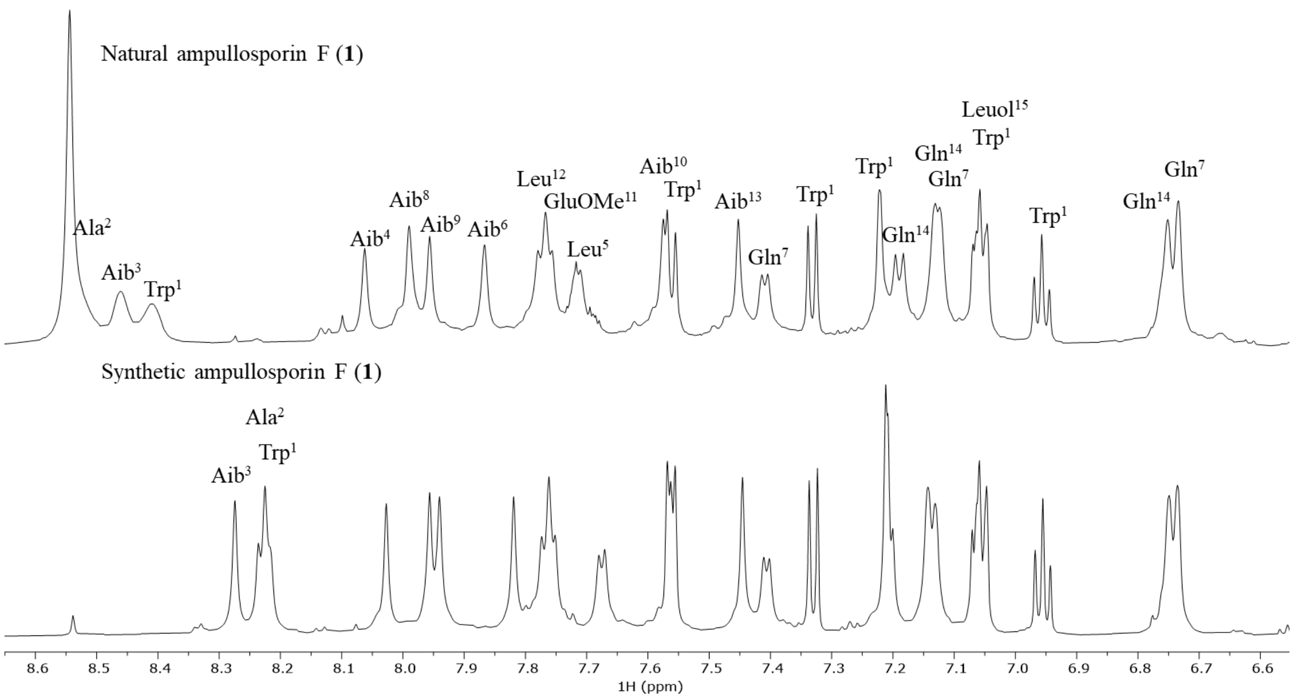

Figure S23. Comparison of the amide and aromatic region in the ^{1}H NMR of natural and synthetic ampullosporin F (**1**) (600 MHz, DMSO-d_6).

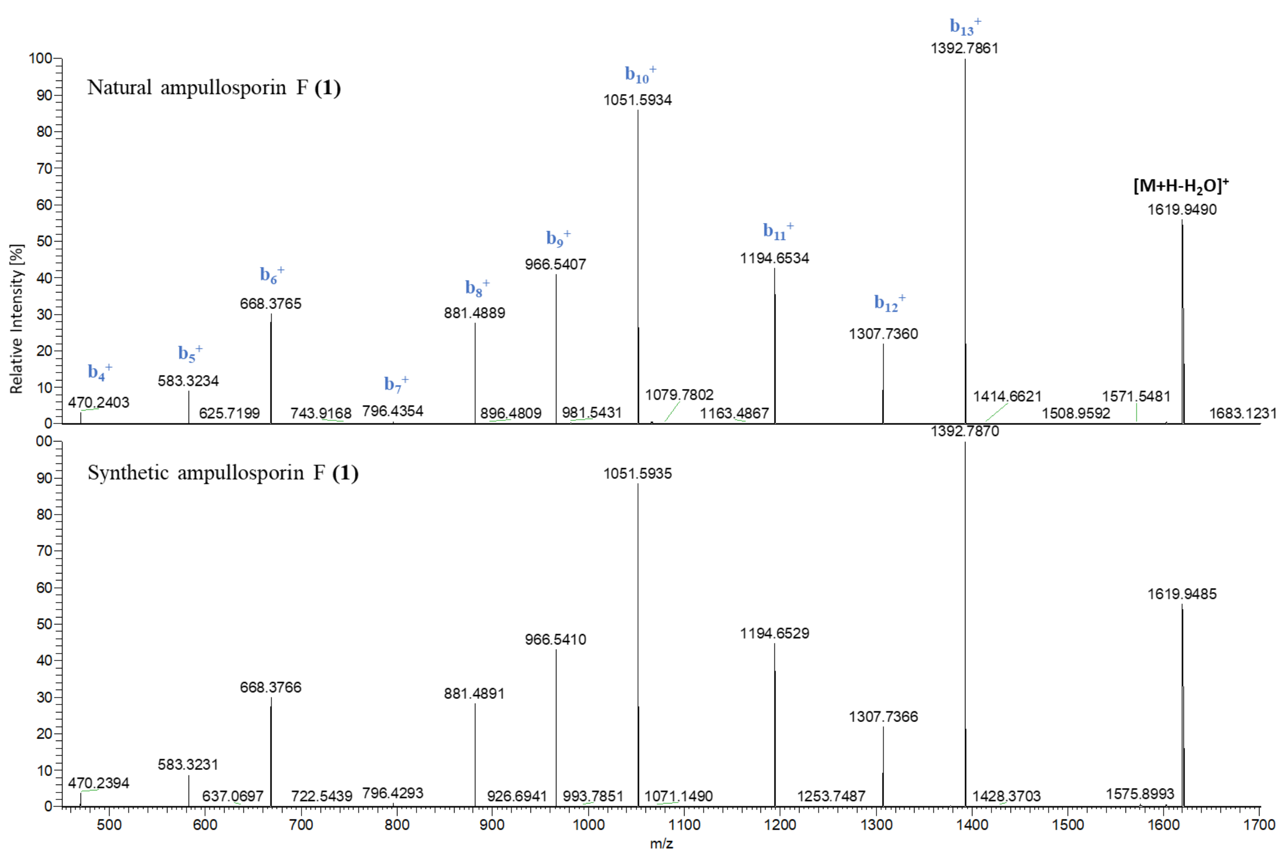

Figure S24. Positive ion MS² spectra of the $[M+H]^+$ of natural and synthetic ampullosporin F (**1**).

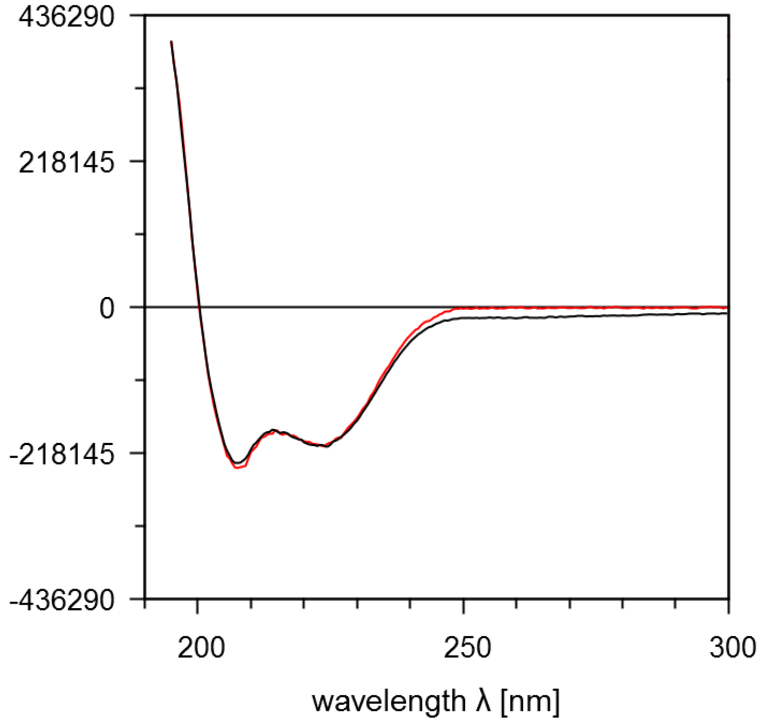

Figure S25. CD spectra of natural (in red) and synthetic (in black) ampullosporin F (**1**) in MeOH.

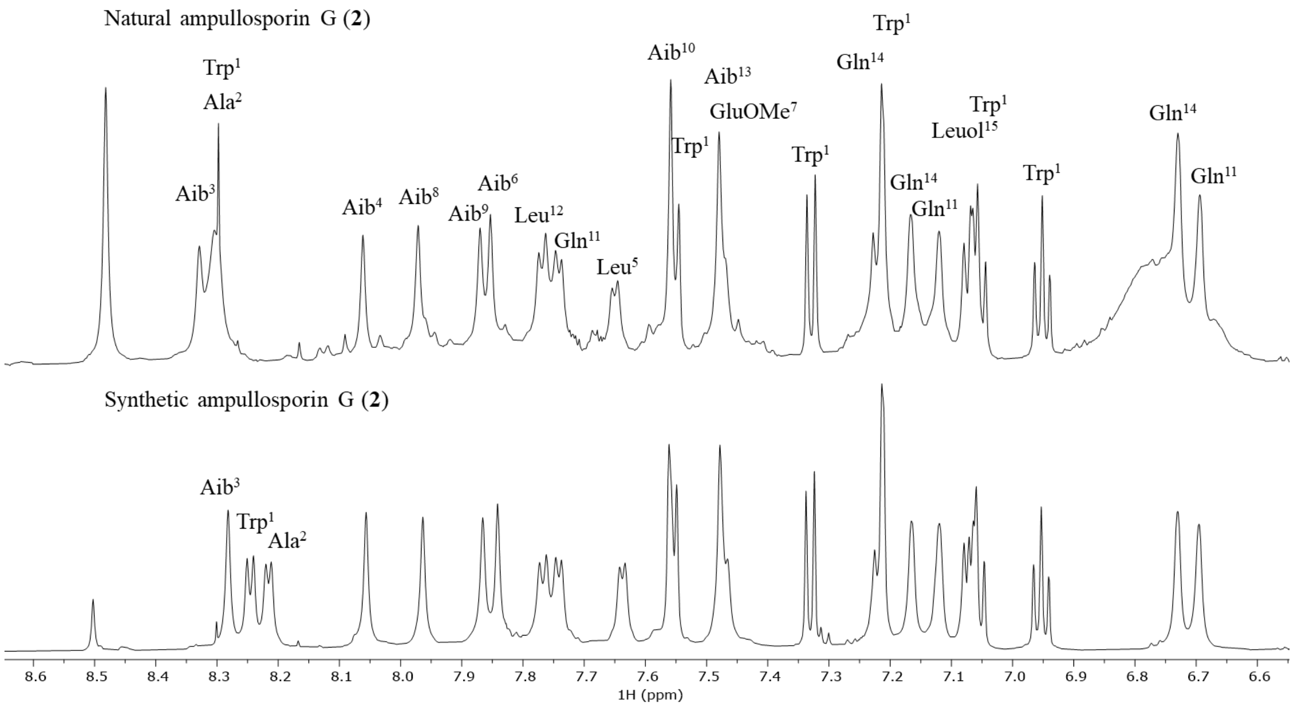

Figure S26. Comparison of the amide and aromatic region in the [1]H NMR of natural and synthetic ampullosporin G (**2**) (600 MHz, DMSO-d_6).

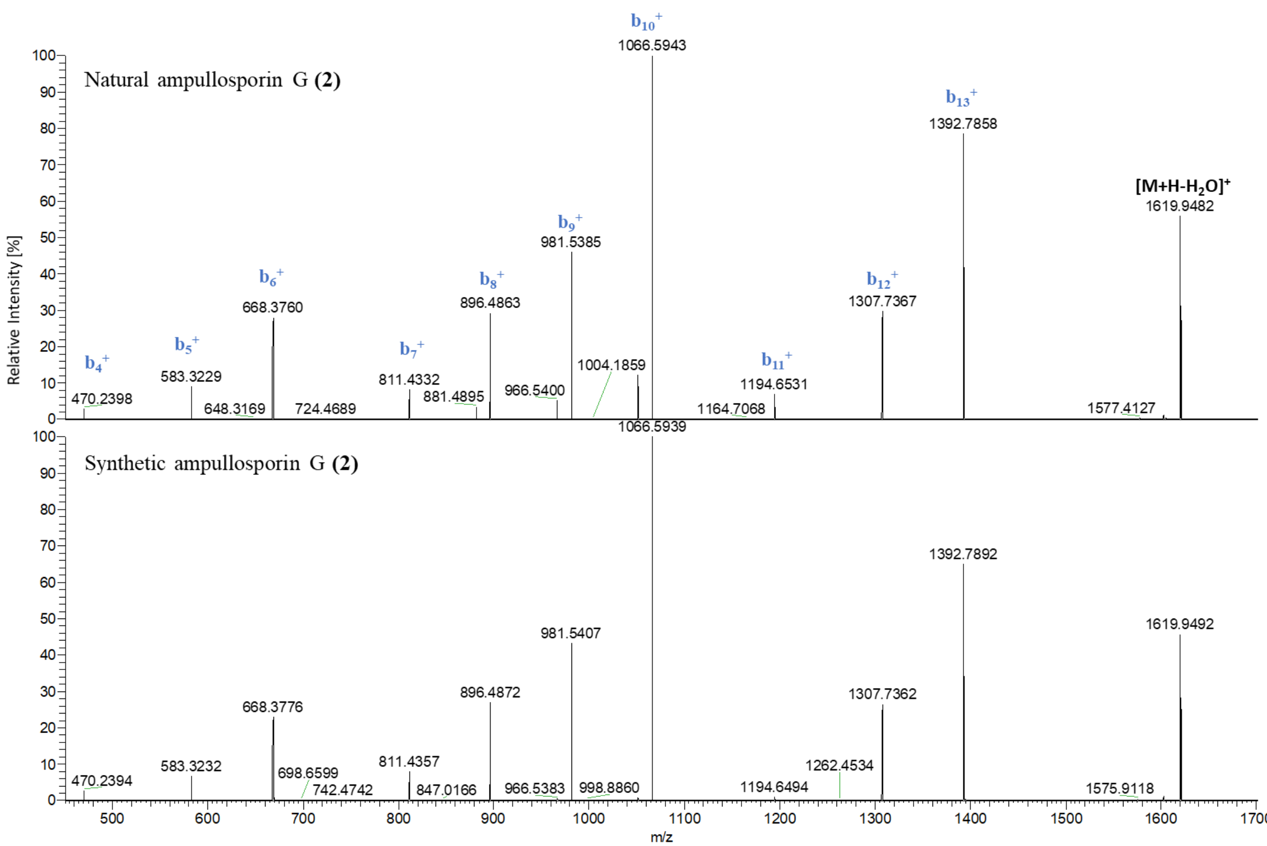

Figure S27. Positive ion MS² spectra of the $[M+H]^+$ of natural and synthetic ampullosporin G (**2**).

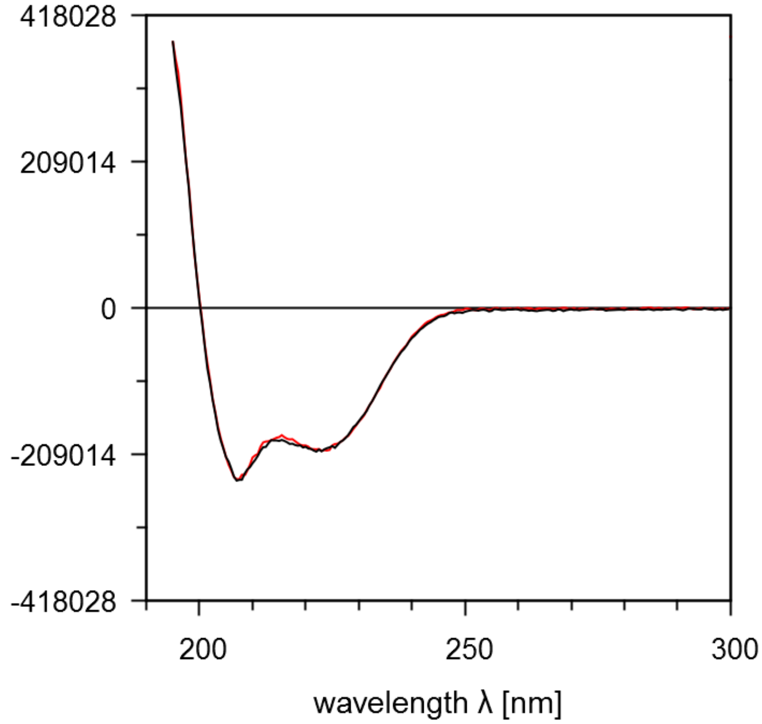

Figure S28. CD spectra of natural (in red) and synthetic (in black) ampullosporin G (**2**) in MeOH.

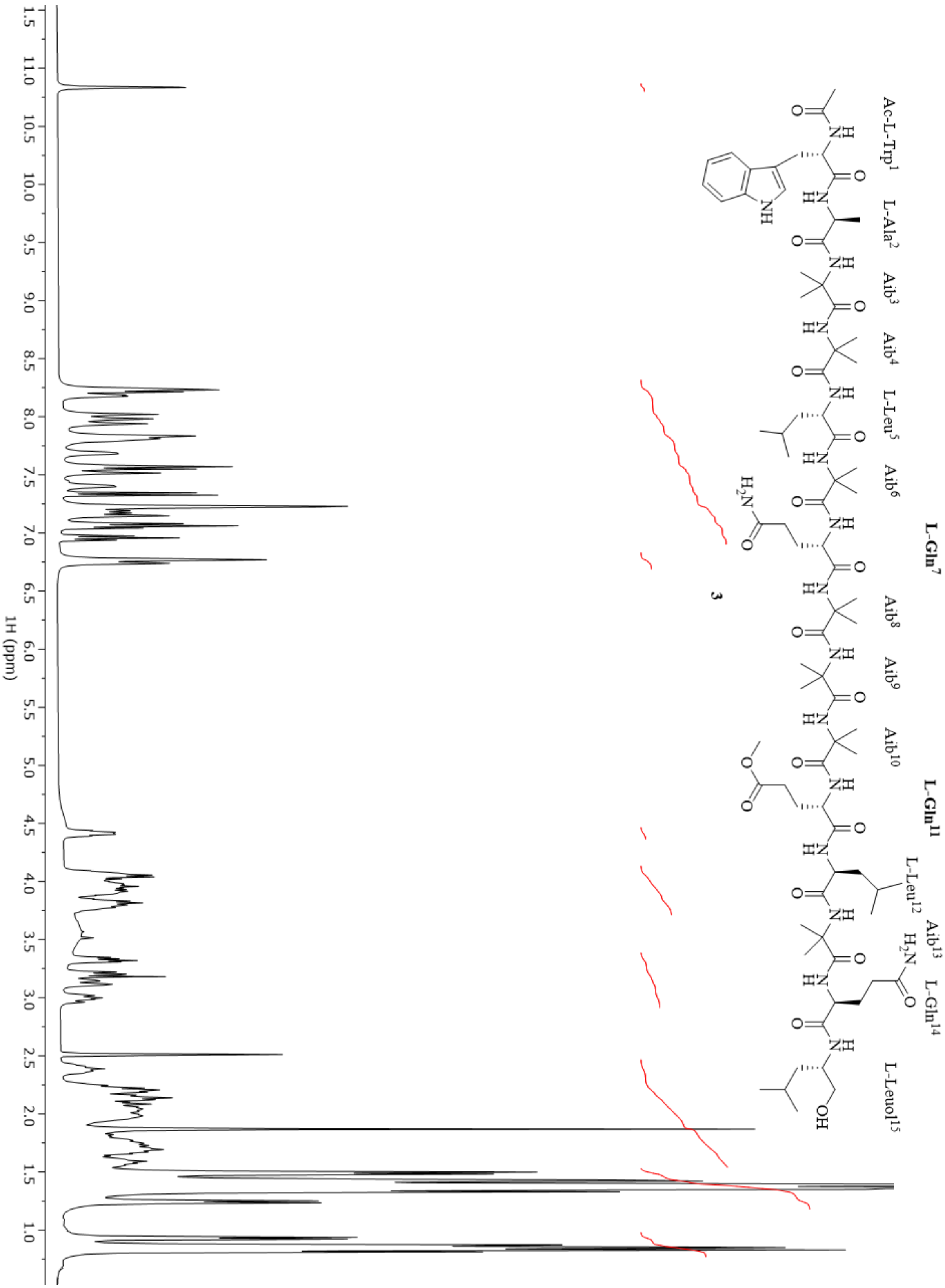

Figure S29. ^{1}H NMR spectrum of natural ampullosporin A (**3**) (400 MHz, DMSO-d_6).

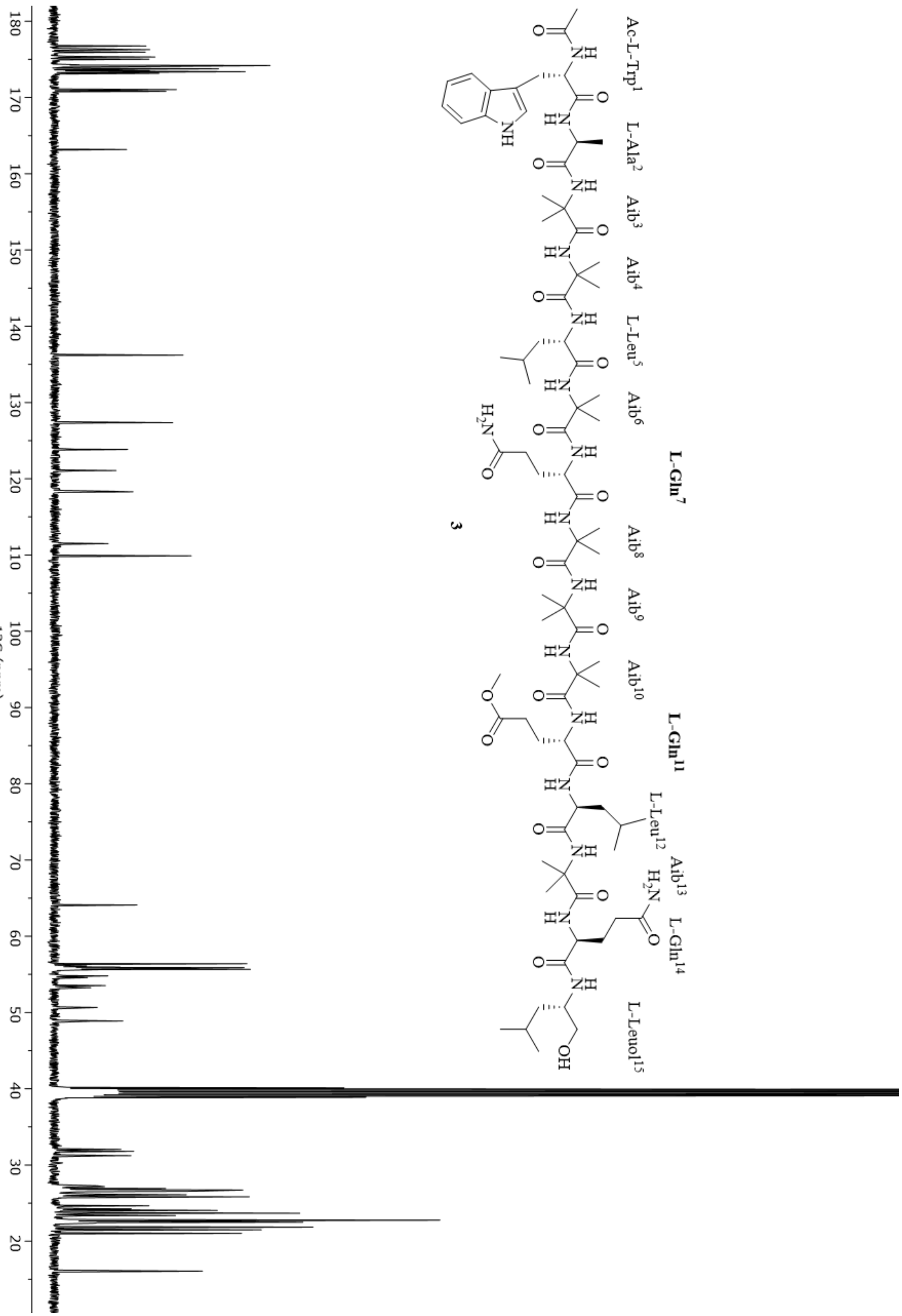

Figure S30. ^{13}C NMR spectrum of natural ampullosporin A (**3**) (100 MHz, DMSO-d_6).

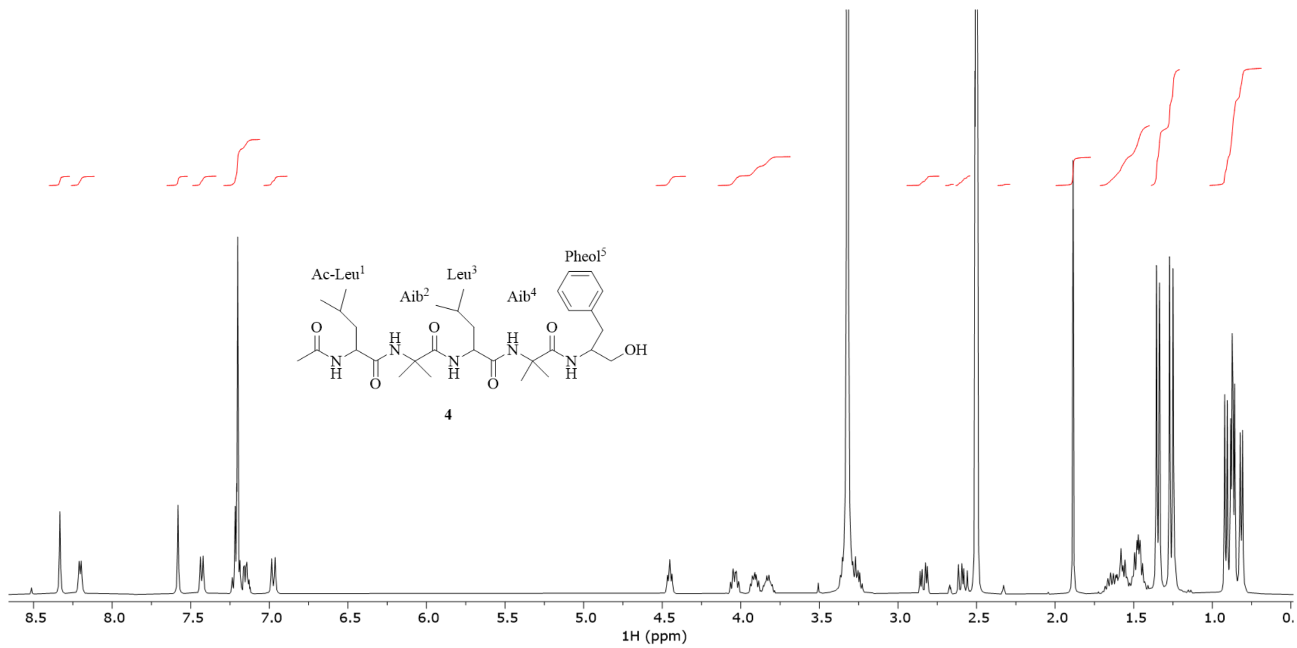

Figure S31. ¹H NMR spectrum of natural peptaibolin (**4**) (400 MHz, DMSO-d_6).

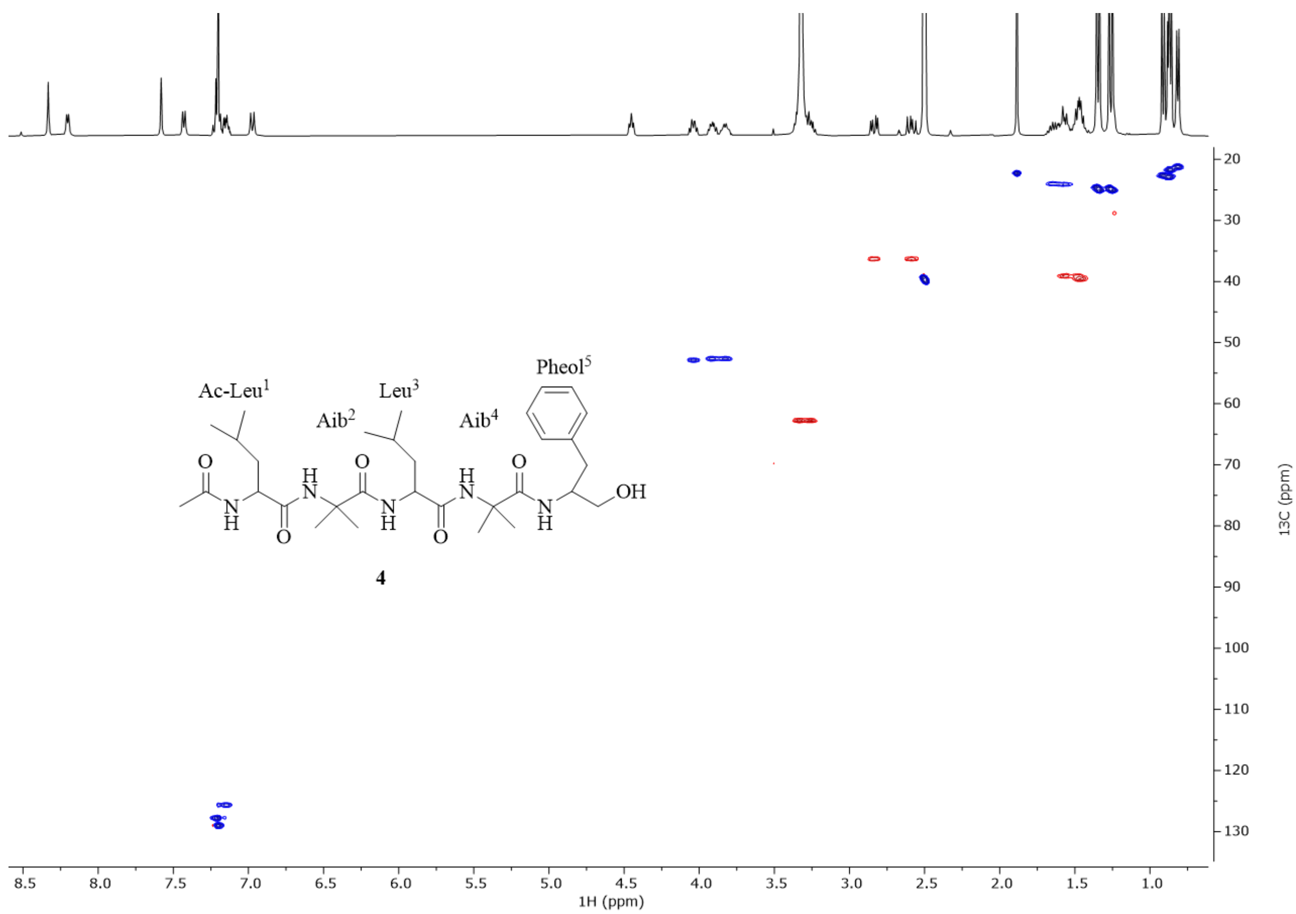

Figure S32. ¹H, ¹³C HSQC spectrum of natural peptaibolin (**4**) (400 MHz, DMSO-d_6).

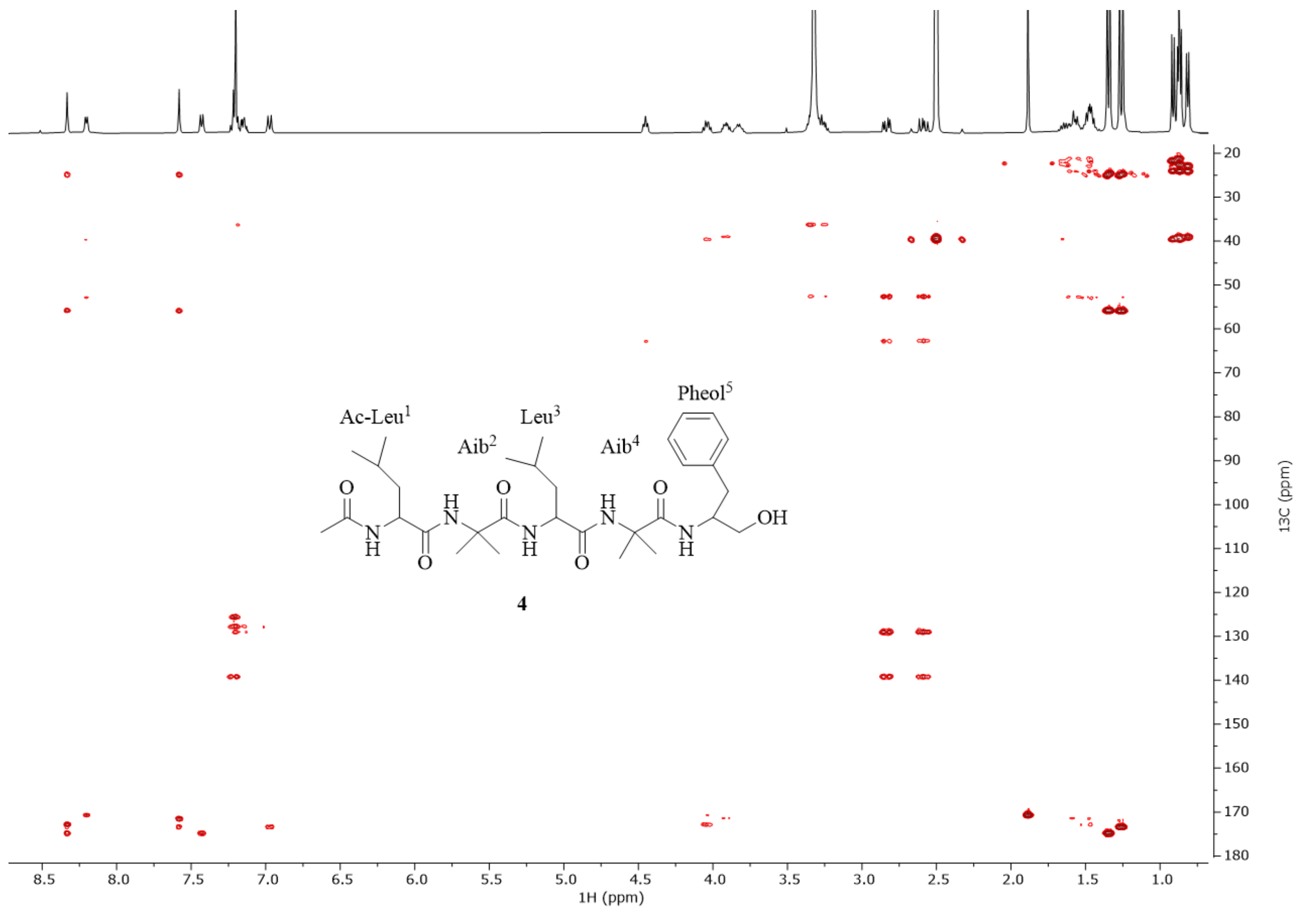

Figure S33. ^{1}H, ^{13}C HMBC spectrum of natural peptaibolin (**4**) (400 MHz, DMSO-d_6).

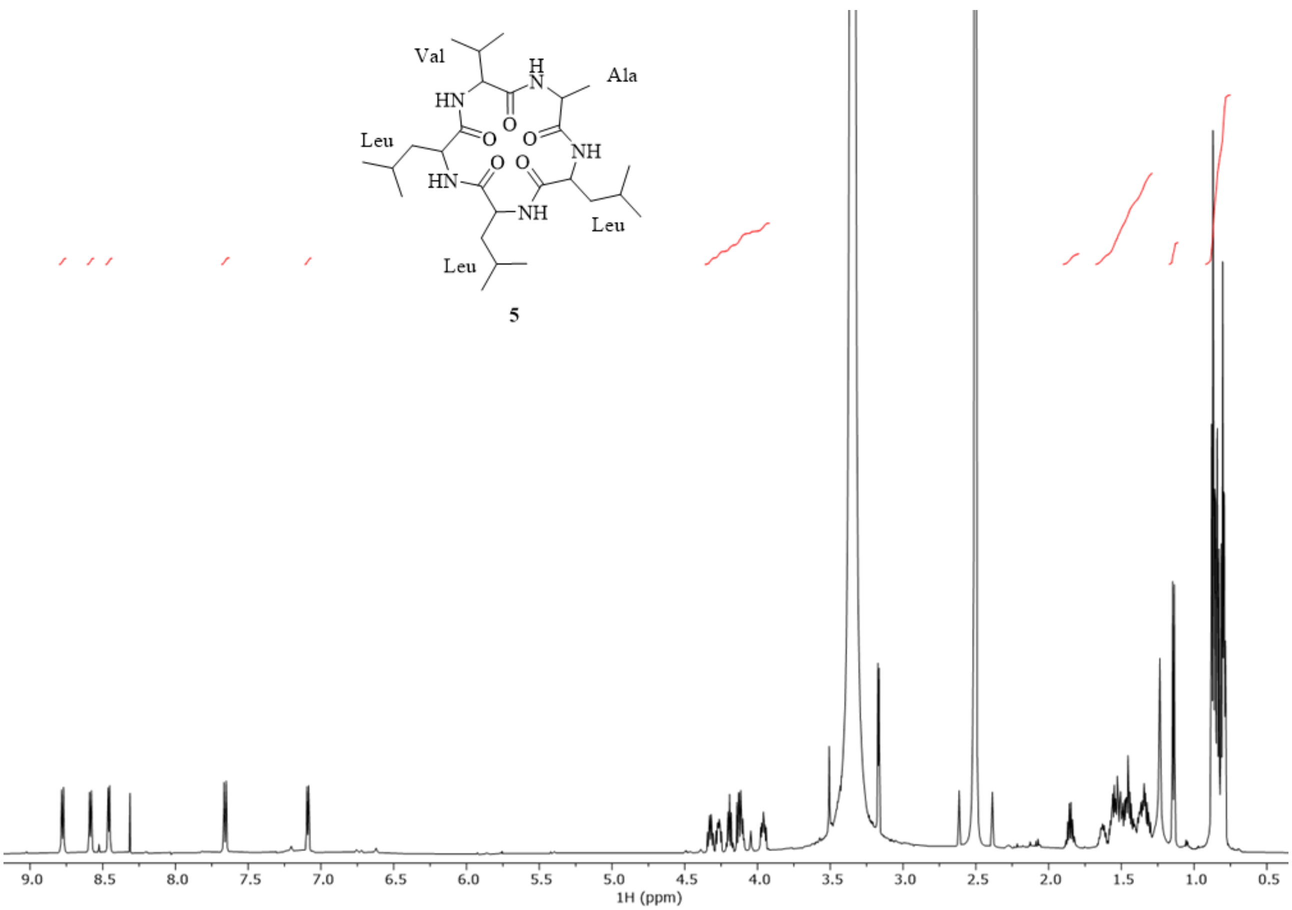

Figure S34. ^{1}H NMR spectrum of natural chrysosporide (**5**) (600 MHz, DMSO-d_6).

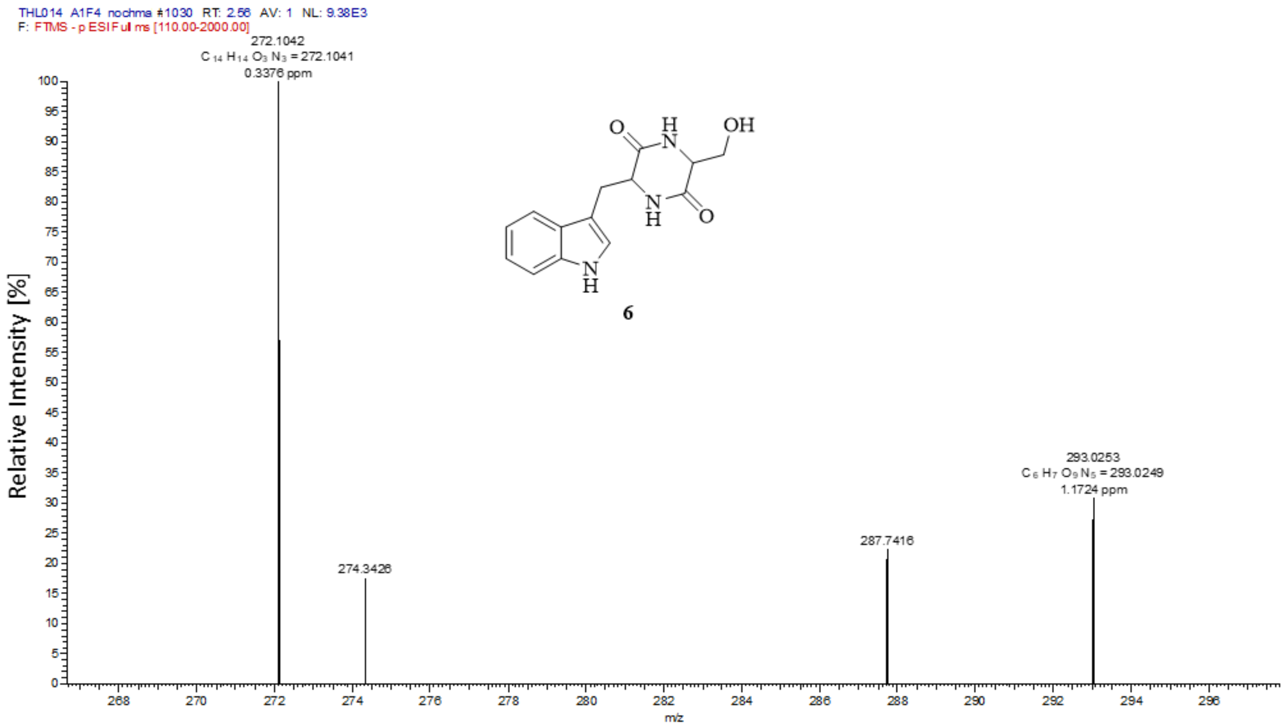

Figure S35. Negative ion mass spectrum of natural c(Trp-Ser) (**6**).

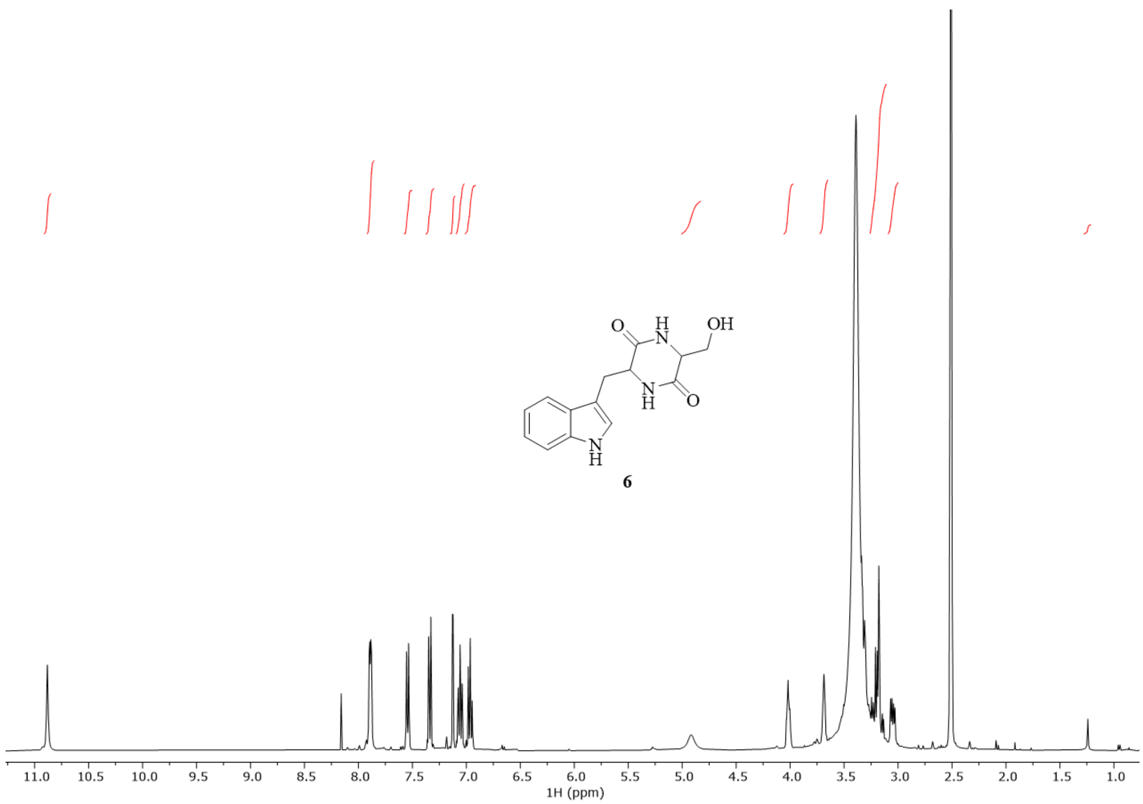

Figure S36. ^{1}H NMR spectrum of natural c(Trp-Ser) (**6**) (400 MHz, DMSO-d_6).

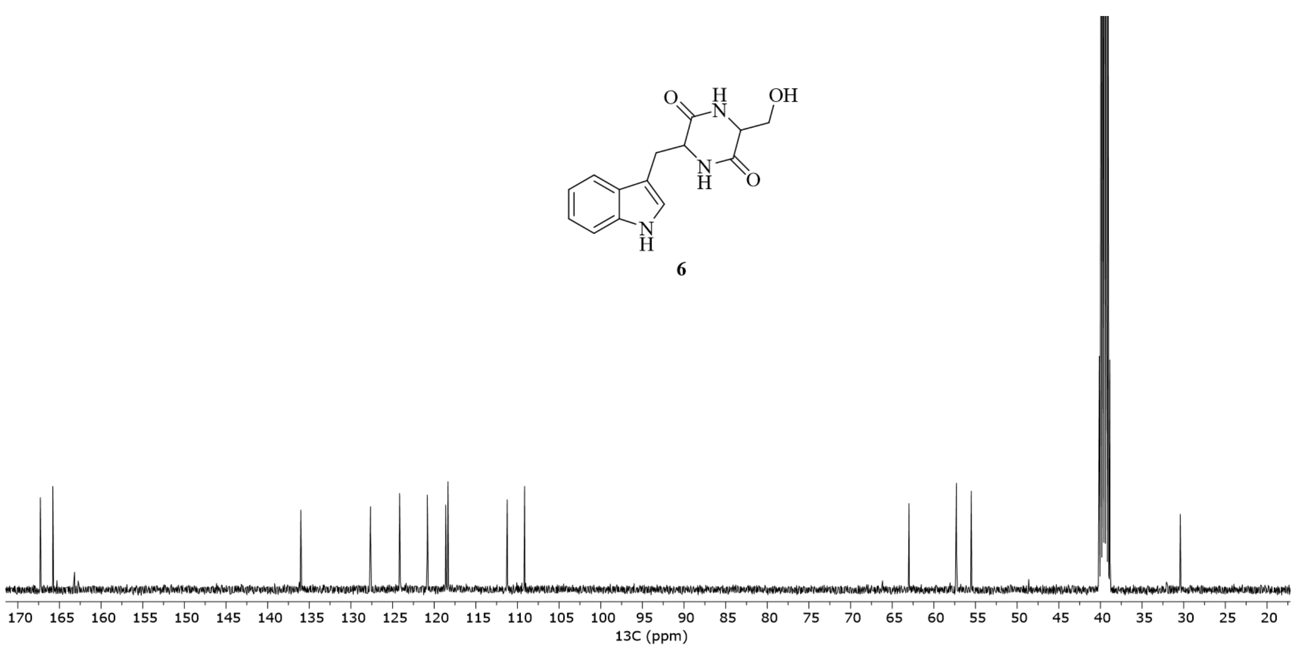

Figure S37. ^{13}C NMR spectrum of natural c(Trp-Ser) (**6**) (100 MHz, DMSO-d_6).

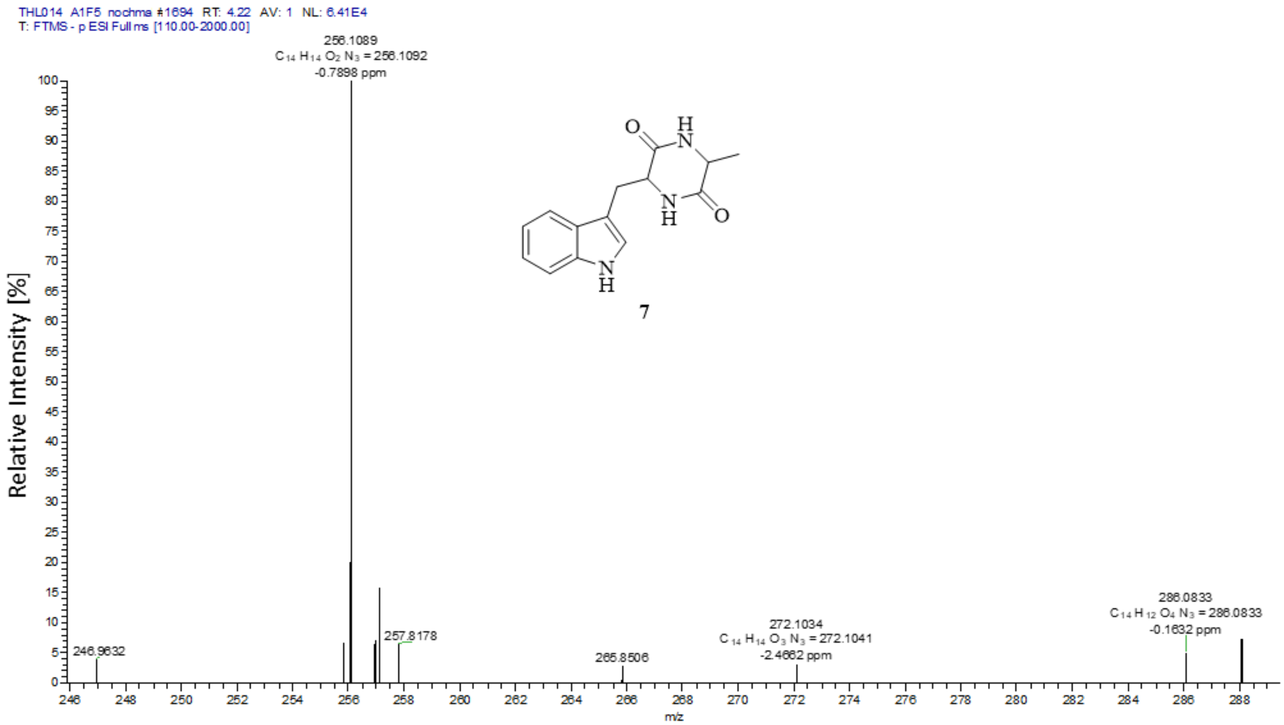

Figure S38. Negative ion mass spectrum of natural c(Trp-Ala) (**7**).

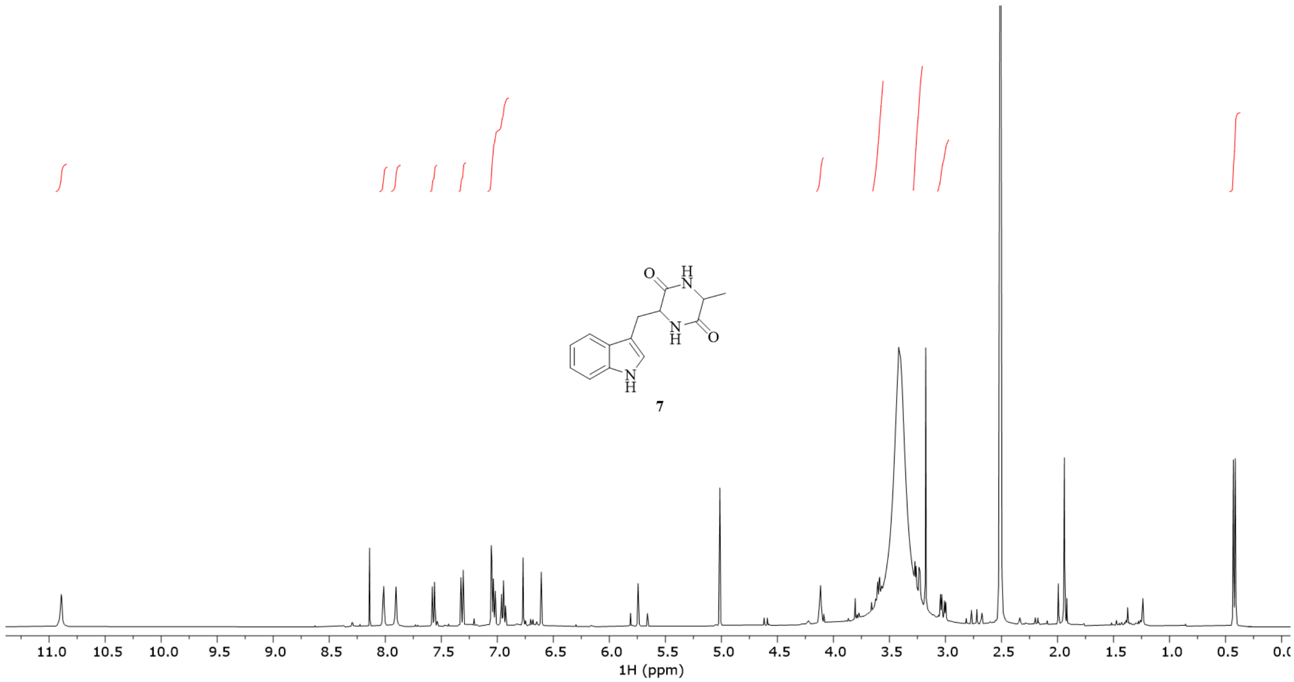

Figure S39. ^{1}H NMR spectrum of natural c(Trp-Ala) (**7**) (400 MHz, DMSO-d_6).

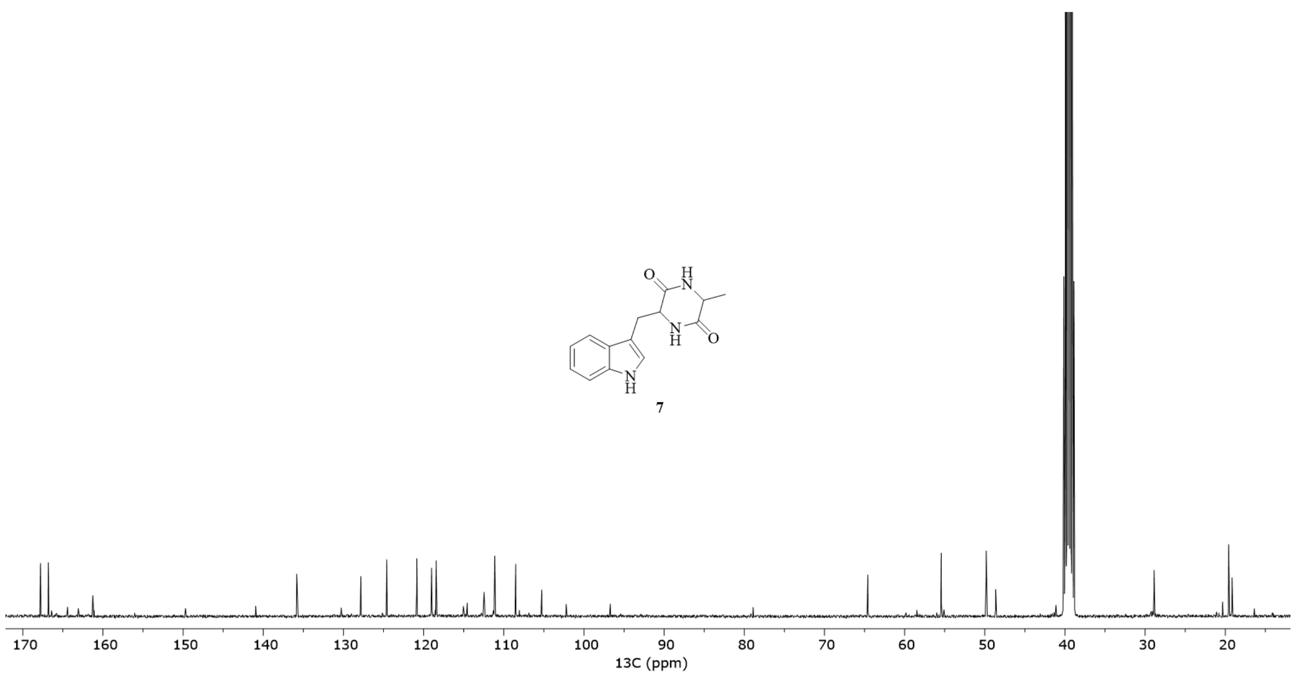

Figure S40. ^{13}C NMR spectrum of natural c(Trp-Ala) (**7**) (100 MHz, DMSO-d_6).

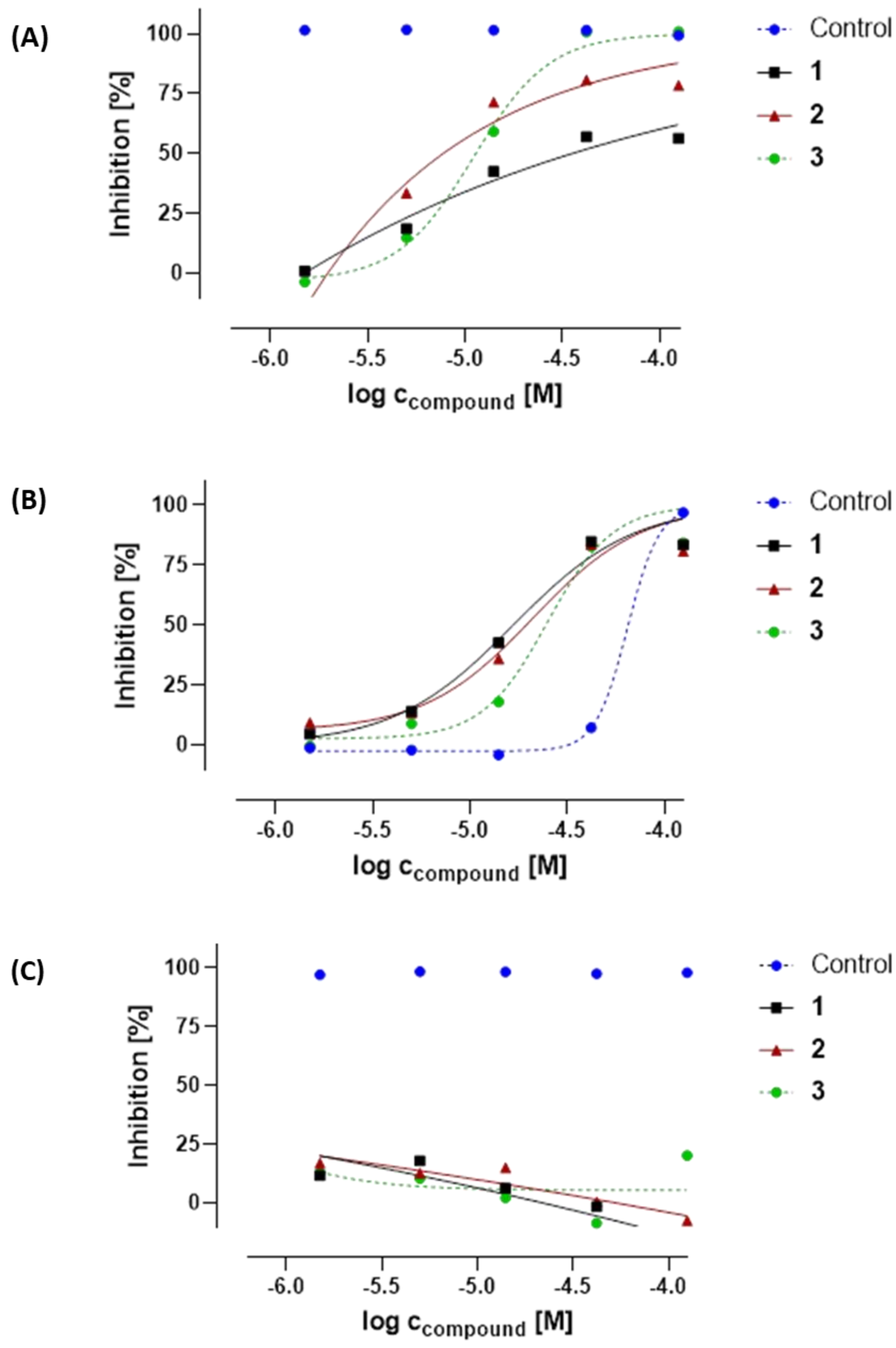

Figure S41 Antiphytopathogenic activity of ampullosporin F (**1**), G (**2**), and A (**3**) against: (**A**) *B. cinerea,* Control = Epoxiconazole; (**B**) *P. infestans,* Control = Terbinafine; and (**C**) *S. tritici,* Control = Epoxiconazole.

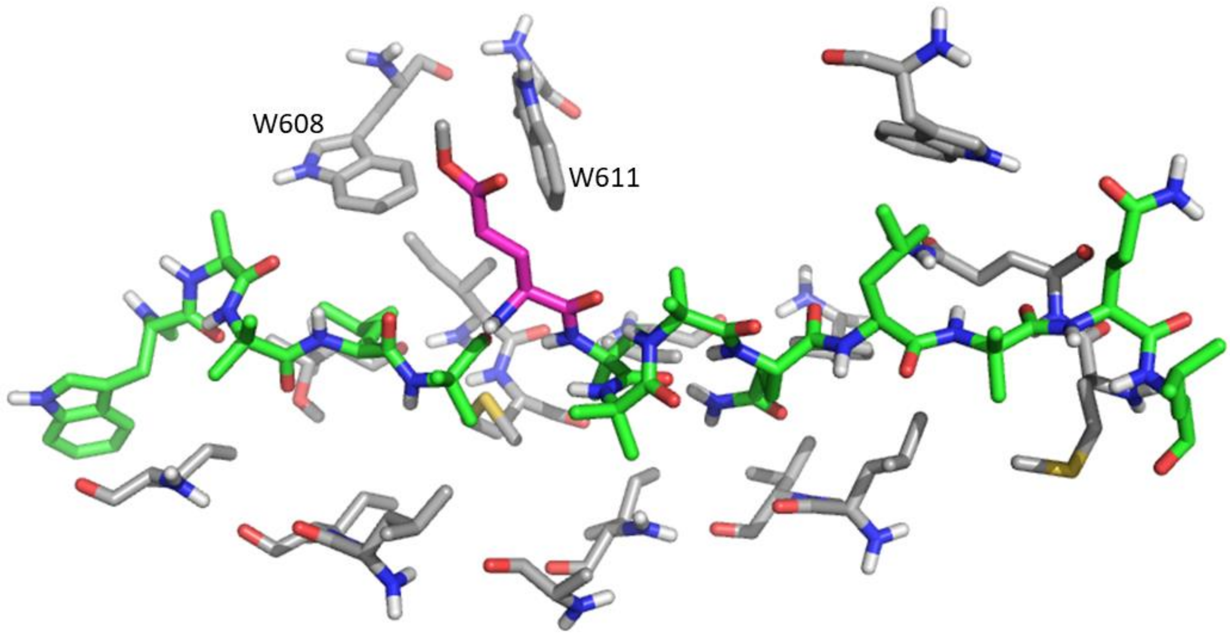

Figure S42 Docking arrangements of ampullosporin G (**2**) in the proposed binding site in the hydrophobic cleft between NMDA receptor subunits GluN1 and GluN2A, as modeled based on protein databank entry 6IRA.

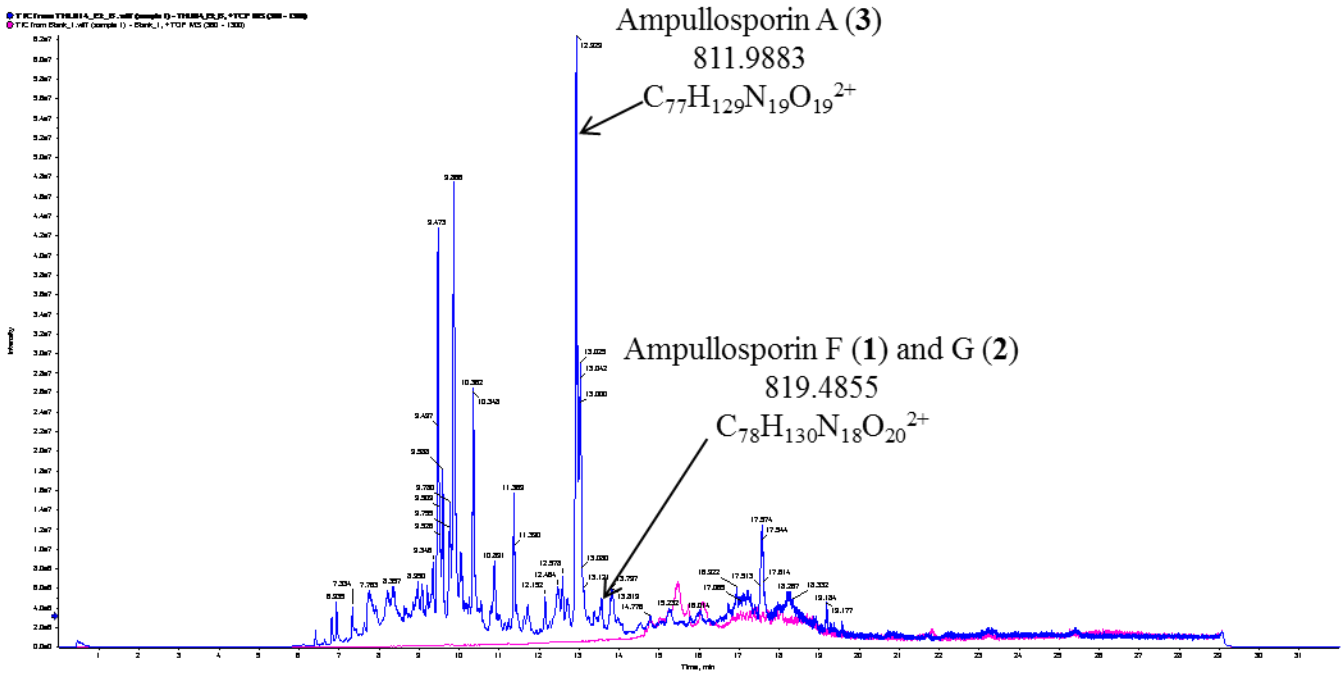

Figure S43. LC-HRMS spectrum of an enriched fraction (in blue) from the ethanol extract of *S. ampullosporum* strain KSH 534 and a blank sample (in pink)

Table S1. Positive and negative ion ESI-HRMS^n data of ampullosporin F (**1**) and G (**2**).

cpd	(+)/(-) scan mode [*m/z* (NCE in%)]	*m/z* (fragment ion, relative intensity in %, error in ppm)
1	(+) full MS	1637.9608 (**[M+H]**$^+$, 14, 1.0), 819.4849 (**[M+2H]**$^{2+}$, 100, 0.0)
	(+) MS^2 [**1638.0** (**35**)]	1619.9515 (**[M+H-H$_2$O]**$^+$, 47, 0.2), 1392.7877 ($\mathbf{b_{13}}^+$, 100, 0.6), 1307.7346 ($\mathbf{b_{12}}^+$, 21, 0.9), 1194.6510 ($\mathbf{b_{11}}^+$, 41, 0.6), 1051.5927 ($\mathbf{b_{10}}^+$, 82, 0.8), 966.5402 ($\mathbf{b_{9}}^+$, 39, 0.6), 881.4879 ($\mathbf{b_{8}}^+$, 25, 0.1), 796.4326 ($\mathbf{b_{7}}^+$, <1, 3.2), 668.3765 ($\mathbf{b_{6}}^+$, 27, 0.2), 583.3235 ($\mathbf{b_{5}}^+$, 7, 0.5), 470.2393 ($\mathbf{b_{4}}^+$, 2, 1.0)
	(+) MS^2 [**819.5** (**30**)]	1392.7917 ($\mathbf{b_{13}}^+$, 8, 3.9), 1194.6517 ($\mathbf{b_{11}}^+$, 8, 0.0), 1168.7280 ($\mathbf{y_{11}}^+$, 11, 1.7), 1055.6453 ($\mathbf{y_{10}}^+$, 17, 0.6), 1051.5925 ($\mathbf{b_{10}}^+$, 35, 0.9), 970.5923 ($\mathbf{y_{9}}^+$, 100, 0.9), 966.5395 ($\mathbf{b_{9}}^+$, 38, 1.3), 881.4879 ($\mathbf{b_{8}}^+$, 41, 0.1), 842.5358 ($\mathbf{y_{8}}^+$, 3, 1.4), 757.4816 ($\mathbf{y_{7}}^+$, 29, 0.2), 672.4281 ($\mathbf{y_{6}}^+$, 25, 1.4), 668.3765 ($\mathbf{b_{6}}^+$, 77, 0.2), 587.3766 ($\mathbf{y_{5}}^+$, 19, 0.9), 583.3242 ($\mathbf{b_{5}}^+$, 16, 0.6), 470.2393 ($\mathbf{b_{4}}^+$, 17, 1.1), 444.3214 ($\mathbf{y_{4}}^+$, <1, 7.6), 385.1870 ($\mathbf{b_{3}}^+$, 6, 0.1), 300.1361 ($\mathbf{b_{2}}^+$, <1, 6.2)
	(+) MS^3 [819.5 (30)→**970.6** (**25**)]	952.5790 ($\mathbf{y_{9}}^+$**-H$_2$O**, 60, 3.8), 853.4770 ($\mathbf{y_{9}}^+$**-aa(15)**, 72, 1.0), 725.4192 ($\mathbf{y_{9}}^+$**-aa(14-15)**, 100, 0.0), 640.3662 ($\mathbf{y_{9}}^+$**-aa(13-15)**, 35, 0.5), 527.2811 ($\mathbf{y_{9}}^+$**-aa(12-15)**, 7, 2.4)
	(+) MS^3 [819.5 (45)→**470.2** (**17**)]	385.1874 ($\mathbf{b_{3}}^+$, 100, 1.2)
	(+) MS^4 [819.5 (45)→470.2 (17) →**385.2** (**17**)]	357.1922 ($\mathbf{b_{3}}^+$**-CO**, 100, 1.1), 300.1345 ($\mathbf{b_{2}}^+$, 86, 0.6)
	(+) MS^5 [819.5 (45)→470.2 (17) →385.2 (17)→**300.1** (**23**)]	229.0977 ($\mathbf{b_{1}}^+$, 100, 1.3)
1	(-) full MS	1681.9465 (**[M-H+HCOOH]**$^-$, 21, 3.5), 1635.9458 (**[M-H]**$^-$, 100, 1.2), 817.4680 (**[M-2H]**$^{2-}$, 11, 2.5)
	(-) MS^2 [**1635.9** (**35**)]	1617.9349 (**[M-H-H$_2$O]**$^-$, 6, 1.5), 1407.8525 ($\mathbf{y_{14}}^-$, 4, 3.9), 1390.7782 ($\mathbf{b_{13}}^-$, <1, 3.0), 1336.8179 ($\mathbf{y_{13}}^-$, 3, 3.0), 1251.7668 ($\mathbf{y_{12}}^-$, 4, 1.1), 1166.7102 ($\mathbf{y_{11}}^-$, 3, 4.6), 1053.6372 ($\mathbf{y_{10}}^-$, 1, 4.1), 1049.5755 ($\mathbf{b_{10}}^-$, 100, 3.3), 968.5731 ($\mathbf{y_{9}}^-$, <1, 5.7), 964.5287 ($\mathbf{b_{9}}^-$, <1, 2.6), 936.5289 ($\mathbf{b_{9}}^-$**-CO**, 66, 2.5), 879.4720 ($\mathbf{b_{8}}^-$, <1, 1.6), 794.4152 ($\mathbf{b_{7}}^-$, <1, 6.9), 666.3598 ($\mathbf{b_{6}}^-$, 2, 3.5), 553.3342 (y_5^-**- CH$_3$OH**, 42, 2.4)
2	(+) full MS	1637.9625 (**[M+H]**$^+$, 15, 0.0), 819.4860 (**[M+2H]**$^{2+}$, 100, 1.4)
	(+) MS^2 [**1638.0** (**35**)]	1619.9508 (**[M+H-H$_2$O]**$^+$, 55, 0.7), 1392.7875 ($\mathbf{b_{13}}^+$, 67, 0.8), 1307.7357 ($\mathbf{b_{12}}^+$, 27, 0.1), 1194.6440 ($\mathbf{b_{11}}^+$, <1, 6.4), 1066.5923 ($\mathbf{b_{10}}^+$, 100, 0.8), 981.5396 ($\mathbf{b_{9}}^+$, 50, 0.8), 896.4871 ($\mathbf{b_{8}}^+$, 32, 0.6), 811.4340 ($\mathbf{b_{7}}^+$, <1, 1.0), 668.3763 ($\mathbf{b_{6}}^+$, 29, 0.4), 583.3235 ($\mathbf{b_{5}}^+$, 10, 0.6), 470.2400 ($\mathbf{b_{4}}^+$, 3, 0.4)
	(+) MS^2 [**819.5** (**30**)]	1520.8486 ($\mathbf{b_{14}}^+$, 2, 3.9), 1392.7886 ($\mathbf{b_{13}}^+$, 39, 0.1), 1307.7392 ($\mathbf{b_{12}}^+$, 2, 2.6), 1194.6516 ($\mathbf{b_{11}}^+$, 5, 0.1), 1168.7295 ($\mathbf{y_{11}}^+$, 8, 0.4), 1066.5919 ($\mathbf{b_{10}}^+$, 82, 1.2),

		1055.6425 (**y_{10}^{+}**, 14, 3.2), 981.5388 (**b_9^{+}**, 88, 1.6), 970.5915 (**y_9^{+}**, 100, 1.7), 896.4869 (**b_8^{+}**, 79, 0.8), 827.5331 (**y_8^{+}**, 2, 2.2), 742.4813 (**y_7^{+}**, 52, 1.1), 668.3763 (**b_6^{+}**, 91, 0.5), 657.4290 (**y_6^{+}**, 62, 0.8), 583.3232 (**b_5^{+}**, 18, 1.2), 572.3767 (**y_5^{+}**, 44, 0.1), 470.2396 (**b_4^{+}**, 17, 0.4), 444.3169 (**y_4^{+}**, 4, 2.7), 385.1872 (**b_3^{+}**, 6, 0.4), 300.1368 (**b_2^{+}**, 1, 8.5), 246.1820 (**y_2^{+}**, 2, 3.3)
	(+) MS^3 [819.5 (30)→**970.6** (**25**)]	952.5803 (**y_9^{+}-H_2O**, 56, 2.4), 853.4765 (**y_9^{+}-aa(15)**, 77, 1.5), 725.4192 (**y_9^{+}-aa(14-15)**, 100, 0.0), 640.3657 (**y_9^{+}-aa(13-15)**, 34, 1.2), 527.2846 (**y_9^{+}-aa(12-15)**, 9, 4.1), 399.2275 (**y_9^{+}-aa(11-15)**, <1, 9.3)
	(+) MS^3 [819.5 (45)→**470.2** (**17**)]	385.1872 (**b_3^{+}**, 100, 0.4)
	(+) MS^4 [819.5 (45)→470.2 (17) →**385.2** (**17**)]	357.1922 (**b_3^{+}-CO**, 100, 0.6), 300.1342 (**b_2^{+}**, 90, 0.3)
	(+) MS^5 [819.5 (45)→470.2 (17) →385.2 (17)→**300.1** (**23**)]	229.0977 (**b_1^{+}**, 100, 2.6)
2	(-) full MS	1681.9472 (**[M-H+HCOOH]$^-$**, 20, 3.7), 1635.9453 (**[M-H]$^-$**, 100, 1.6), 817.4681 (**[M-2H]$^{2-}$**, 7, 2.7)
	(-) MS^2 [**1635.9** (**35**)]	1617.9287 (**[M-H-H_2O]$^-$**, <1, 5.4), 1407.8543 (**y_{14}^{-}**, <1, 2.7), 1390.7803 (**b_{13}^{-}**, <1, 4.5), 1336.8093 (**y_{13}^{-}**, <1, 8.7), 1251.7572 (**y_{12}^{-}**, <1, 8.8), 1192.6478 (**b_{11}^{-}**, <1, 8.9), 1166.7143 (**y_{11}^{-}**, 3, 1.0), 1064.5835 (**b_{10}^{-}**, <1, 8.9), 1053.6284 (**y_{10}^{-}**, 1, 2.8), 968.5767 (**y_9^{-}**, <1, 1.3), 936.5499 (**y_9^{-}- CH_3OH**, 100, 2.7), 825.5215 (y_8^{-}, <1, 1.4), 740.4655 (y_7^{-}, 3, 2.9), 666.3651 (**b_6^{-}**, <1, 4.5), 655.4136 (y_6^{-}, 3, 1.8), 570.3615 (y_5^{-}, 2, 1.1), 553.3342 (y_5^{-}**- NH_3**, 3, 2.4)

Table S2. Positive ion ESI-HRMS^n data of ampullosporin A (**3**), peptaibolin (**4**) and chrysosporide G (**5**).

cpd	(+)/(-) scan mode [*m/z* (NCE in%)]	*m/z* (fragment ion, relative intensity in %, error in ppm)
3	(+) full MS	1622.9628 ($\mathbf{[M+H]^+}$, 52, 0.0), 811.9851 ($\mathbf{[M+2H]^{2+}}$, 100, 0.1)
	(+) MS^2 [**1623.0** (**45**)]	1604.9509 ($\mathbf{[M+H\text{-}H_2O]^+}$, 94, 0.8), 1377.7959 ($\mathbf{b_{13}}^+$, 15, 5.1), 1292.7404 ($\mathbf{b_{12}}^+$, 29, 3.3), 1051.5931 ($\mathbf{b_{10}}^+$, 51, 0.3), 966.5410 ($\mathbf{b_9}^+$, 45, 0.2), 881.4872 ($\mathbf{b_8}^+$, 56, 0.9), 668.3757 ($\mathbf{b_6}^+$, 100, 1.4), 583.3231 ($\mathbf{b_5}^+$, 34, 1.3), 470.2400 ($\mathbf{b_4}^+$, 16, 0.5)
	(+) MS^2 [**812.0** (**45**)]	1377.7928 ($\mathbf{b_{13}}^+$, 16, 2.9), 1292.7458 ($\mathbf{b_{12}}^+$, 1, 7.5), 1153.7329 ($\mathbf{y_{11}}^+$, 8, 2.2), 1051.5951 ($\mathbf{b_{10}}^+$, 39, 1.5), 1040.6482 ($\mathbf{y_{10}}^+$, 13, 1.9), 966.5419 ($\mathbf{b_9}^+$, 36, 1.2), 955.5953 ($\mathbf{y_9}^+$, 83, 1.9), 881.4892 ($\mathbf{b_8}^+$, 36, 1.4), 742.4830 ($\mathbf{y_7}^+$, 34, 1.1), 668.3775 ($\mathbf{b_6}^+$, 100, 1.3), 657.4302 ($\mathbf{y_6}^+$, 25, 1.3), 583.3246 ($\mathbf{b_5}^+$, 42, 1.2), 572.3776 ($\mathbf{y_5}^+$, 24, 1.7), 470.2406 ($\mathbf{b_4}^+$, 46, 1.6), 444.3177 ($\mathbf{y_4}^+$, 4, 0.9), 385.1878 ($\mathbf{b_3}^+$, 21, 2.0), 331.2343 ($\mathbf{y_3}^+$, <1, 1.0), 300.1360 ($\mathbf{b_2}^+$, 3, 5.6), 246.1816 ($\mathbf{y_2}^+$, 2, 1.7), 229.0992 ($\mathbf{b_1}^+$, <1, 9.1)
4	(+) full MS	590.3892 ($\mathbf{[M+H]^+}$, 100, 3.4)
	(+) MS^2 [**590.4** (**35**)]	572.3789 ($\mathbf{[M+H\text{-}H_2O]^+}$, 27, 3.1), 439.2899 ($\mathbf{b_4}^+$, 100, 3.5), 354.2377 ($\mathbf{b_3}^+$, 18, 2.8), 241.1542 ($\mathbf{b_2}^+$, 4, 2.1)
5	(+) full MS	510.3649 ($\mathbf{[M+H]^+}$, 100, 0.2), 532.3468 ($\mathbf{[M+Na]^+}$, 28, 0.2)
	(+) MS^2 [**510.4** (**35**)]	492.3546 ($\mathbf{[M+H\text{-}H_2O]^+}$, 10, 0.3), 482.3700 ($\mathbf{[M+H\text{-}CO]^+}$, 90, 0.2), 465.3435 ($\mathbf{[M+H\text{-}CO\text{-}NH_3]^+}$, 43, 0.2), 411.2961 ($\mathbf{b_{4AV}}$, 85, 1.1), 397.2806 ($\mathbf{b_{4LL}/b_{4LL}*/b_{4VL}}$, 100, 0.8), 383.3018 ($\mathbf{a_{4AV}}$, 12, 0.4), 369.2861 ($\mathbf{a_{4LL}/a_{4LL}*/a_{4VL}}$, 26, 0.3), 366.2754 ($\mathbf{[a_{4AV}\text{-}NH_3]^+}$, 4, 0.8), 352.2596 ($\mathbf{[a_{4LL}/a_{4LL}*/a_{4VL}\text{-}NH_3]^+}$, 9, 0.5), 340.2596 ($\mathbf{b_{3LA}}$, 2, 0.5), 326.2433 ($\mathbf{b_{3LL}}$, 4, 1.5), 298.2127 ($\mathbf{b_{3AV}}$, 23, 0.6), 284.1970 ($\mathbf{b_{3LL}*/b_{3VL}}$, 18, 0.5), 227.1757 ($\mathbf{b_{2LA}/b_{2LL}}$, 3, 1.5), 213.1600 ($\mathbf{b_{2LL}*}$, 1, 1.3), 199.1807 ($\mathbf{a_{2LL}/a_{2LA}}$, 2, 1.1), 185.1647 ($\mathbf{a_{2LL}*}$, 1, 1.0), 185.1286 ($\mathbf{b_{2AV}}$, 1, 0.9), 171.1125 ($\mathbf{b_{2VL}}$, <1, 1.7), 157.1337 ($\mathbf{a_{2AV}}$, 1, 0.8)